and A21–178 in Chiba University. Doxorubicin (10 mg/kg body weight) was intraperitoneally injected into wild-type male mice (C57BL/6) once-weekly at weeks 7 and 8 after birth. After both Doxorubicin injections, the mice were reared for a further 2 weeks, and the surviving mice were used for experiments. Myocardial infarction models were prepared using wild-type male mice (C57BL/6) as previously described [11]. Serum and Gr-1(+) cells were isolated 4 weeks after inducing myocardial infarction (11 weeks of age).

Generation of EGFRdn mice. The C-terminal 533 amino acids [42] were deleted from the full-length human *EGFR* cDNA (a gift from Professor T. Kadowaki, The University of Tokyo) by introducing a stop codon (TGA) after the R677 codon by site-directed mutagenesis. The truncated *EGFR* (*EGFRdn*) cDNA was then subcloned into the *αMHC* promoter-containing expression vector (a gift from Professor J. Robbins, Cincinnati Children's Hospital). The 8.2-kb DNA fragment was microinjected as a transgene into pronuclei of eggs from BDF1 mice. The eggs were then transferred into the oviducts of pseudopregnant ICR mice. The transgenic founders were identified by Southern blot and PCR analysis. Line 2–5 and Line 9–12 were established and maintained by breeding to C57BL/6 mice. Line 9–12 was selected for further analysis on the basis of a higher level of transgene expression.

BMMNC infusion and CM injection. BMMNC (2.0×10^7) isolated from a male wild-type mouse and suspended in 200 μl of PBS or an equal volume of PBS as a control were injected into the tail veins of anesthetized (4% inhaled isoflurane) 8-week-old male EGFRdn mice and 11-week-old male DOX and OMI mice. CM (200 μl) from Gr-1(+) cells from male wild-type mice or isovolume serum-depleted DMEM were infused into the tail veins of anesthetized 8-week-old male EGFRdn mice and 11-week-old male DOX mice under anesthesia. Anti-mouse insulin-like growth factor-1 (IGF-1) (0.1 μg/g body weight) or anti-goat immunoglobulin G (IgG) (0.1 μg/g body weight) antibodies were intraperitoneally injected into 11-week-old male DOX mice 2 h before CM infusion. Anti-activin A (20 μg) or anti-mouse IgG (20 μg) antibodies were intraperitoneally injected at 48-h intervals into male EGFRdn mice from 10 to 12 weeks of age. Pegvisomant (10 mg/kg body weight) or vehicle (control) were intraperitoneally injected into 8-week-old male DOX mice 30 min before CM infusion.

Evaluation of cell shortening and the beating rate of cardiomyocytes. After 12 h starvation with 500 μl serum-depleted DMEM in 12-well dishes, rat cardiomyocytes were cultured with 500 μl of CM or serum-depleted DMEM. At specific times, the cultured cardiomyocytes were video recorded for 10 sec, and the percentage of cell shortening was analyzed using ImageExpress version 5.5 (Nippon Roper). To measure the percentage of cell shortening, two regions of interest were fixed by the software, which analyzed the beating distance of a single cardiomyocyte, and divided the distance by the length between the regions of interest. The number of beats of single cardiomyocyte was counted for 10 sec to determine the beating rate. For antibody treatment *in vitro*, the starved cardiomyocytes were pretreated with anti-IGF-1 (10 μg/ml) or anti-goat IgG (10 μg/ml) antibodies for 2 h before adding CM. For pegvisomant treatment *in vitro*, the cardiomyocytes were pretreated with pegvisomant (12.5 μg/ml) for 30 min before adding CM.

Echocardiography and catheterization. Transthoracic echocardiographic analysis and catheterization analysis were performed as previously described [11]_ENREF_9. Briefly, the +dp/dt in the left ventricle was measured using a catheter, which was introduced retrogradely *via* the carotid artery.

Cell isolation. Neonatal rat cardiomyocytes were isolated and separately collected as described previously [43]. Cardiomyocytes were plated at a density of 1×10^5 cells/cm^2 on six-, 12- and 24-well dishes (BD Falcon) coated with 1% gelatin and cultured in DMEM supplemented with 10% FBS. Adult cardiomyocytes were prepared as previously described [44]. BMMNC and PBMNC were isolated from 8-week-old male C57BL/6, male GFP mice, and male EGFRdn mice by density gradient centrifugation with Histopaque-1083, as previously described [45]. PBMNC were also isolated from human subjects, as previously described [46].

Sorting of harvested BMMNC into sub-populations and collection of CM. After BMMNC were harvested from male wild-type mice, the cells were sorted into Gr-1(+) cells, B220(+) cells, TER(+) cells, and lineage-negative populations using a Magnetic Cell Sorting system (Miltenyi Biotec), as previously described [47]. To collect the CM, the individual sub-populations were seeded onto 24-well dishes with 200 μl of serum-depleted DMEM. After incubation for 24 h in serum-depleted DMEM, the supernatant (CM) was collected, and any cells were removed by filtering through a 0.45-μm filter (BD Falcon).

Phase-contrast live imaging. Live images of beating cardiomyocytes were taken using a Leica inverted microscope (Leica) equipped with a phase-contrast objective and a CCD camera (Leica).

Flow cytometry. The percentage of cells expressing each cell surface antigen was analyzed using a FACSCalibur (Becton Dickinson Immunocytometry Systems) and Cell Quest Pro version 5.2 software.

RNA extraction and DNA microarray analysis. Total RNA was extracted from 12-week-old male wild-type ($n=4$) and age-matched male EGFRdn mice ($n=4$) using a RNeasy Mini Kit (Qiagen) according to the manufacturer's protocol. RNA quality was assessed with an Agilent 2100 Bioanalyzer (Agilent Technologies). cRNA preparation, fragmentation, hybridization, and scanning of a GeneChip® Mouse Genome 430 2.0 Arrays (Affymetrix) were performed according to the manufacturer's protocol. cRNA was labeled using a Two-cycle Eukaryotic Target Labeling assay with a GeneChip Expression 3′ amplification two-cycle labeling and control reagents kit (Affymetrix). Briefly, cDNA was generated from total RNA (100 ng) using SuperScript II (Invitrogen) and a T7-oligo(dT) promoter primer (Affymetrix). After second-strand cDNA synthesis, cDNA was converted to cRNA by an *in vitro* transcription reaction (MEGAscript T7 kit, Ambion). The cRNA was then purified using a Sample Cleanup Module (Affymetrix), and the yield was monitored with a spectrophotometer. The second cycle of cDNA synthesis was performed, followed by the same cleanup as above and a second *in vitro* transcription reaction cycle with biotin-labeled ribonucleotides and T7 RNA polymerase. The labeled cRNA was purified, using a Sample Cleanup Module and denatured at 94°C before hybridization. The samples were hybridized to GeneChip® Mouse Genome 430 2.0 Arrays at 45°C for 16 h with rotation at 60 rpm. The arrays were then washed, stained with phycoerythrin–streptavidin (Molecular Probes), washed, and scanned with a GeneChip Scanner 3000 7G (Affymetrix). The data were analyzed with GeneSpring version 7.3.1 software (Agilent Technologies).

Reverse transcriptase-PCR. RNA extraction and RT-PCR were performed as previously described [11]. Real-time PCR amplification was performed using an Applied Biosystems 7500 real-time PCR system (Applied Biosystems) with QuantiTect SYBR Green PCR Master Mix (Qiagen). The PCR protocol comprised an initial denaturation step (94°C, 15 sec) followed by 60 cycles of amplification and quantification (55°C for 30 sec and 72°C for 35 sec) and a melting curve program (60–95°C). The

relative mRNA expression level was calculated using the standard curve of GAPDH. All samples were independently analyzed at least three times for each gene. Semi-quantitative RT-PCR of GH was performed using 0.4 μg of total RNA and followed by 40 cycles of the above conditions. The primer sequences were QT00311654 (Qiagen) for GH in real-time PCR, 5′-TCCTGTGGACAGATCACTGC-3′ and 5′-AATGTAGGCACGCTCGAACT-3′ for GH in semi-quantitative PCR, QT00309099 (Qiagen) for GAPDH, and 5′-GGACCTGGCTGGCCGGGACC-3′ and 5′-GCGGTGCACGATGGAGGGGC-3′ for β-actin. For semi-quantitative RT-PCR, the PCR products were size-fractionated by 2% agarose gel electrophoresis.

Northern blot analysis. For northern blot analysis, total RNA (20 μg) was extracted from hearts using TRIzol Reagent (Invitrogen) and hybridized with a cDNA probe for *EGFRdn*. 18S rRNA ethidium bromide staining was used to quantify RNA loading.

Analysis of phosphorylated ErbB receptor expression. Four-week-old mice were anesthetized by intraperitoneal injection of urethane (2 mg/g body weight) followed by intravenous injection of HB-EGF (0.5 μg/g body weight, R&D Systems), NRG-1β (0.5 μg/g body weight, R&D Systems), or vehicle *via* the inferior vena cava. After 5 min, the hearts were immediately excised and homogenized in a buffer containing 50 mmol/l HEPES (pH 7.5), 137 mmol/l NaCl, 1 mmol/l $MgCl_2$, 1 mmol/l $CaCl_2$, 10 mmol/l Na-pyrophosphate, 2 mmol/l EDTA, 1% NP-40, 10% glycerol, 2 mmol/l Na_3VO_4, 10 mmol/l NaF, and protease inhibitor cocktail (Complete Mini, Roche Applied Science). To analyze the tyrosine phosphorylation of ErbB receptors, equivalent amounts of proteins were subjected to immunoprecipitation with the specific antibodies, fractionated by 6% SDS-PAGE, and immunoblotted with the mouse monoclonal anti-phosphotyrosine antibody 4G10 (Millipore). Horseradish peroxidase-conjugated anti-mouse IgG antibody (GE Healthcare) was used as the secondary antibody, and the bound antibodies were detected using an ECL detection kit (GE Healthcare).

ELISA. Serum and CM concentrations of cAMP, GH and activin A were measured by ELISA (cAMP and activin A, R&D Systems; GH, LINCO Research). To prepare cell lysates for cAMP analysis, cardiomyocytes were seeded (4×10^5 cells/cm) onto six-well dishes coated with 1% gelatin and cultured in DMEM supplemented with 10% FBS. After 5 d, the cells were washed three times with PBS and the medium was changed to serum-depleted DMEM. After incubation for 12 h in the serum-depleted medium, the cells were washed three times with PBS and the medium was replaced with 1 ml of serum-depleted DMEM with CM (1 ml), 2 ml of serum-depleted DMEM with 500 pg/ml GH, 2 ml of serum-depleted DMEM with 12.5 μg/ml pegvisomant, or 1 ml of serum-depleted DMEM plus 1 ml of CM and 12.5 μg/ml pegvisomant. Thirty minutes later, the cardiomyocytes were resuspended in lysis buffer in six-well dish.

To examine the expression of NFκB and phosphorylated NFκB in PBMNC, PBMNC isolated from wild-type male mice were cultured with AngII or TNFα. Thirty minutes later, PBMNC were resuspended in lysis buffer and the expression of NFκB and phosphorylated NFκB were examined using sandwich ELISA kits (Cell Signaling). Some cells were also treated with 50 μM NFκB p65 (Ser276) inhibitory peptide to inhibit NFκB activity.

Western blot analysis. Whole-cell lysates (30–50 μg) were resolved by SDS-PAGE. The separated proteins were transferred to a PVDF membrane (GE Healthcare) and incubated with the primary antibody, followed by an anti-IgG-horseradish peroxidase-conjugated secondary antibody. Proteins were detected using an ECL-Plus kit (GE Healthcare).

Immunohistology. The hearts were fixed with 4% paraformaldehyde and embedded in paraffin, or fixed in 10% neutralized formalin and embedded in Tissue-Tek OCT cryo-embedding compound (Sakura Finetek). The specimens were sectioned (5 μm thick), and stained with hematoxylin/eosin or Masson trichrome.

Evaluation of cardiac hypertrophy. To evaluate the mean diameter of LV cardiomyocytes, the shortest diameter of each cardiomyocyte was measured in nucleated transverse sections stained with hematoxylin-eosin. Thirty cardiomyocytes in each LV were measured using an ocular micrometer disc with a linear scale at a magnification of 400×, and the average cardiomyocyte diameter was calculated for each specimen. Four hearts were measured in each group. The cell surface area of isolated neonatal and adult cardiomyocytes was measured by planimetry in 50 randomly selected cells per specimen.

Immunofluorescence staining. Immunostaining was performed as previously described [45]. Images were taken using a fluorescent microscopy (Leica) with LAS AF software (Leica).

Human subjects. We enrolled 10 subjects who were outpatients of Department of Cardiology of Tokyo Women's Medical University Hospital. We obtained 10 ml of whole blood from each patient. Half of the blood sample was used to measure the serum activin A concentration and the remaining blood was used to measure GH in CM after PBMNC isolation. All patients were receiving medical therapies and exhibited New York Heart Association class II symptoms. We also enrolled 11 healthy age- and body mass index-matched volunteers. Characteristics of the patients and healthy subjects are summarized in Table S1.

Statistics. Data are presented as means ± s.e.m. We examined differences between groups by Student's *t* test or analysis of variance followed by Bonferroni's correction to compare means. A value of $P<0.05$ was considered to be significant.

Supporting Information

Figure S1 Overexpression of EGFRdn inhibited the functional activation of endogenous ErbB receptors in a dominant-negative manner. (A) Northern blot analysis for the transgene expression in hearts from wild-type and two different founder lines of EGFRdn mice (L2–5 and L9–12). (B) Tyrosine phosphorylation of ErbB receptors in hearts from wild-type and EGFRdn mice (L9–12) at 5 min after injection of HB-EGF. In wild-type mice, intravenous injection of HB-EGF enhanced cardiac tyrosine phosphorylation of EGFR, ErbB2 and ErbB4, which was abrogated in EGFRdn hearts. HB-EGF, heparin-binding EGF-like growth factor. (C) Tyrosine phosphorylation of ErbB receptors in hearts from wild-type and EGFRdn mice (L9–12) at 5 min after the injection of NRG-1β. NRG-1β induced tyrosine phosphorylation of ErbB2 and ErbB4 in wild-type hearts, but not in EGFRdn hearts. NRG-1, neuregulin-1.
(TIF)

Figure S2 Echocardiographic analysis of DOX mice. (A) Representative M-mode images of wild-type and DOX mice. (B) Left ventricular diastolic and systolic dimensions, and FS of 11-week-old DOX mice ($n=36$) and age-matched wild-type mice ($n=10$). LVDd, left ventricular diastolic dimension; LVDs, left ventricular systolic dimension. Data are means ± s.e.m.
(TIF)

Figure S3 Analysis of cardiac hypertrophy. (A) The shortest diameter of each cardiomyocyte ($n=30$ per group). Lower photographs, H&E-stained tissue sections. Scale bar, 75 μm. (B) Surface area of isolated adult cardiomyocytes ($n=50$ per group).

Lower photographs, representative images. Scale bar, 75 μm. Data are means ± s.e.m.
(TIF)

Figure S4 Flow cytometric analysis. The left and right panels show the expression of each cell surface marker before and after magnetic sorting (MACS), respectively.
(TIF)

Figure S5 Cardiac hypertrophy *in vitro*. Upper graph, cell surface area of neonatal rat cardiomyocytes ($n = 50$); lower photographs, representative images of the cells. Cardiomyocytes were stained with sarcomeric α-actinin (red). Nuclei were stained with Hoechst 33258 (blue). Scale bars, 75 μm. Data are means ± s.e.m.
(TIF)

Figure S6 Comparison of GH concentration. GH concentration in CM from Gr-1(+) cells isolated from old myocardial infarction (OMI) mice and DOX mice ($n = 5$). Data are means ± s.e.m.
(TIF)

Figure S7 BMMNC improve the cardiac function of OMI mice via the GH receptor. (A) At 4 weeks after coronary ligation, BMMNC were infused via the tail vein. Pegvisomant (10 mg/kg body weight) or vehicle (control) was intraperitoneally injected into OMI mice 30 min before infusing BMMNC. BMMNC infusion improved FS and +dp/dt at 3 d after infusion and these improvements were inhibited by pegvisomant (n = 5). (B) Masson trichrome staining. Panels show representative images. Scale bars: 1 mm. Data are means ± s.e.m.
(TIF)

Figure S8 Direct effects of GH in the CM from Gr-1(+) cells on cardiomyocytes. CM from Gr-1(+) cells from wild-type mice was infused into DOX-treated wild-type mice (wild-DOX) or DOX-treated cardiac-specific STAT3dn mice (STAT3dn-DOX). Gr-1(+) cell-derived CM improved FS (left) and +dp/dt (right) in wild-DOX mice ($n = 5$) at 1 d after infusion, but not in STAT3dn-DOX ($n = 5$). Data are means ± s.e.m.
(TIF)

Figure S9 Serum activin A concentrations ($n = 5$). Data are means ± s.e.m.
(TIF)

Figure S10 TNFα increases the secretion of activin A from PBMNC *via* NFκB. (A) Activin A levels in CM from PBMNC were upregulated by treatment with TNFα ($n = 5$). (B) TNFα (50 ng/ml) activated NFκB in PBMNC ($n = 5$). Left, total NFκB; right, phosphorylated NFκB. (C) TNFα (50 ng/ml) -mediated upregulation of activin A in PBMNC was inhibited by treatment with the NFκB inhibitory peptide ($n = 5$). Isotype peptide was used as control. Data are means ± s.e.m.
(TIF)

Table S1 Characteristics of human subjects.
(PDF)

Acknowledgments

We thank M. Okabe (Osaka University, Japan) for the GFP transgenic mice, K. Yamauchi-Takihara (Osaka University) for the cardiac-specific STAT3dn mice, N. Ueno (Tokyo Women's Medical University) for manuscript preparation, T. Kadowaki (The University of Tokyo, Tokyo), J. Robbins (Children's Hospital, Cincinnati, OH) for providing cDNAs, A. Suzuki and K. Nomura (Tokyo Women's Medical University) for their technical supports, and H. Nagao and K. Yoshihara for their excellent technical assistance.

Author Contributions

Conceived and designed the experiments: KM IK. Performed the experiments: NF KM HA AH TN TT AS KMM. Analyzed the data: NF KM HA. Contributed reagents/materials/analysis tools: TS TO. Wrote the paper: NF KM NH IK.

References

1. Passier R, van Laake LW, Mummery CL (2008) Stem-cell-based therapy and lessons from the heart. Nature 453: 322–329.
2. Schachinger V, Erbs S, Elsasser A, Haberbosch W, Hambrecht R, et al. (2006) Intracoronary bone marrow-derived progenitor cells in acute myocardial infarction. N Engl J Med 355: 1210–1221.
3. Segers VF, Lee RT (2008) Stem-cell therapy for cardiac disease. Nature 451: 937–942.
4. van Ramshorst J, Bax JJ, Beeres SL, Dibbets-Schneider P, Roes SD, et al. (2009) Intramyocardial bone marrow cell injection for chronic myocardial ischemia: a randomized controlled trial. JAMA 301: 1997–2004.
5. Martin-Rendon E, Brunskill SJ, Hyde CJ, Stanworth SJ, Mathur A, et al. (2008) Autologous bone marrow stem cells to treat acute myocardial infarction: a systematic review. Eur Heart J 29: 1807–1818.
6. Donndorf P, Kundt G, Kaminski A, Yerebakan C, Liebold A, et al. (2011) Intramyocardial bone marrow stem cell transplantation during coronary artery bypass surgery: A meta-analysis. J Thorac Cardiovasc Surg.
7. Orlic D, Kajstura J, Chimenti S, Jakoniuk I, Anderson SM, et al. (2001) Bone marrow cells regenerate infarcted myocardium. Nature 410: 701–705.
8. Murry CE, Soonpaa MH, Reinecke H, Nakajima H, Nakajima HO, et al. (2004) Haematopoietic stem cells do not transdifferentiate into cardiac myocytes in myocardial infarcts. Nature 428: 664–668.
9. Cho HJ, Lee N, Lee JY, Choi YJ, Ii M, et al. (2007) Role of host tissues for sustained humoral effects after endothelial progenitor cell transplantation into the ischemic heart. J Exp Med 204: 3257–3269.
10. Gnecchi M, He H, Liang OD, Melo LG, Morello F, et al. (2005) Paracrine action accounts for marked protection of ischemic heart by Akt-modified mesenchymal stem cells. Nat Med 11: 367–368.
11. Matsuura K, Honda A, Nagai T, Fukushima N, Iwanaga K, et al. (2009) Transplantation of cardiac progenitor cells ameliorates cardiac dysfunction after myocardial infarction in mice. J Clin Invest 119: 2204–2217.
12. Muller AF, Kopchick JJ, Flyvbjerg A, van der Lely AJ (2004) Clinical review 166: Growth hormone receptor antagonists. J Clin Endocrinol Metab 89: 1503–1511.
13. Funamoto M, Fujio Y, Kunisada K, Negoro S, Tone E, et al. (2000) Signal transducer and activator of transcription 3 is required for glycoprotein 130-mediated induction of vascular endothelial growth factor in cardiac myocytes. J Biol Chem 275: 10561–10566.
14. Bodner M, Castrillo JL, Theill LE, Deerinck T, Ellisman M, et al. (1988) The pituitary-specific transcription factor GHF-1 is a homeobox-containing protein. Cell 55: 505–518.
15. Ingraham HA, Chen RP, Mangalam HJ, Elsholtz HP, Flynn SE, et al. (1988) A tissue-specific transcription factor containing a homeodomain specifies a pituitary phenotype. Cell 55: 519–529.
16. Gaddy-Kurten D, Vale WW (1995) Activin increases phosphorylation and decreases stability of the transcription factor Pit-1 in MtTW15 somatotrope cells. J Biol Chem 270: 28733–28739.
17. Yndestad A, Ueland T, Oie E, Florholmen G, Halvorsen B, et al. (2004) Elevated levels of activin A in heart failure: potential role in myocardial remodeling. Circulation 109: 1379–1385.
18. Schrier RW, Abraham WT (1999) Hormones and hemodynamics in heart failure. N Engl J Med 341: 577–585.
19. Takahashi M, Suzuki E, Takeda R, Oba S, Nishimatsu H, et al. (2008) Angiotensin II and tumor necrosis factor-alpha synergistically promote monocyte chemoattractant protein-1 expression: roles of NF-kappaB, p38, and reactive oxygen species. Am J Physiol Heart Circ Physiol 294: H2879–2888.
20. Gao LR, Wang ZG, Zhu ZM, Fei YX, He S, et al. (2006) Effect of intracoronary transplantation of autologous bone marrow-derived mononuclear cells on outcomes of patients with refractory chronic heart failure secondary to ischemic cardiomyopathy. Am J Cardiol 98: 597–602.
21. Bartke A (2005) Minireview: role of the growth hormone/insulin-like growth factor system in mammalian aging. Endocrinology 146: 3718–3723.
22. Giustina A, Lorusso R, Borghetti V, Bugari G, Misitano V, et al. (1996) Impaired spontaneous growth hormone secretion in severe dialated cardiomyopathy. Am Heart J 131: 620–622.
23. Colligan PB, Brown-Borg HM, Duan J, Ren BH, Ren J (2002) Cardiac contractile function is enhanced in isolated ventricular myocytes from growth hormone transgenic mice. J Endocrinol 173: 257–264.
24. Tajima M, Weinberg EO, Bartunek J, Jin H, Yang R, et al. (1999) Treatment with growth hormone enhances contractile reserve and intracellular calcium

transients in myocytes from rats with postinfarction heart failure. Circulation 99: 127–134.
25. Bueno OF, De Windt LJ, Tymitz KM, Witt SA, Kimball TR, et al. (2000) The MEK1-ERK1/2 signaling pathway promotes compensated cardiac hypertrophy in transgenic mice. EMBO J 19: 6341–6350.
26. Shiojima I, Sato K, Izumiya Y, Schiekofer S, Ito M, et al. (2005) Disruption of coordinated cardiac hypertrophy and angiogenesis contributes to the transition to heart failure. J Clin Invest 115: 2108–2118.
27. Matsui T, Li L, del Monte F, Fukui Y, Franke TF, et al. (1999) Adenoviral gene transfer of activated phosphatidylinositol 3′-kinase and Akt inhibits apoptosis of hypoxic cardiomyocytes in vitro. Circulation 100: 2373–2379.
28. Kunisada K, Negoro S, Tone E, Funamoto M, Osugi T, et al. (2000) Signal transducer and activator of transcription 3 in the heart transduces not only a hypertrophic signal but a protective signal against doxorubicin-induced cardiomyopathy. Proc Natl Acad Sci U S A 97: 315–319.
29. Harada M, Qin Y, Takano H, Minamino T, Zou Y, et al. (2005) G-CSF prevents cardiac remodeling after myocardial infarction by activating the Jak-Stat pathway in cardiomyocytes. Nat Med 11: 305–311.
30. Sirotkin AV (2005) Control of reproductive processes by growth hormone: extra- and intracellular mechanisms. Vet J 170: 307–317.
31. Colao A, Vitale G, Pivonello R, Ciccarelli A, Di Somma C, et al. (2004) The heart: an end-organ of GH action. Eur J Endocrinol 151: S93–101.
32. Colao A (2008) The GH-IGF-I axis and the cardiovascular system: clinical implications. Clin Endocrinol 69: 347–358.
33. Welch S, Plank D, Witt S, Glascock B, Schaefer E, et al. (2002) Cardiac-specific IGF-1 expression attenuates dilated cardiomyopathy in tropomodulin-overexpressing transgenic mice. Circ Res 90: 641–648.
34. Torella D, Rota M, Nurzynska D, Musso E, Monsen A, et al. (2004) Cardiac stem cell and myocyte aging, heart failure, and insulin-like growth factor-1 overexpression. Circ Res 94: 514–524.
35. Marleau S, Mulumba M, Lamontagne D, Ong H (2006) Cardiac and peripheral actions of growth hormone and its releasing peptides: relevance for the treatment of cardiomyopathies. Cardiovasc Res 69: 26–35.
36. Le Corvoisier P, Hittinger L, Chanson P, Montagne O, Macquin-Mavier I, et al. (2007) Cardiac effects of growth hormone treatment in chronic heart failure: A meta-analysis. J Clin Endocrinol Metab 92: 180–185.
37. Cicoira M, Kalra PR, Anker SD (2003) Growth hormone resistance in chronic heart failure and its therapeutic implications. J Card Fail 9: 219–226.
38. Anker SD, Chua TP, Ponikowski P, Harrington D, Swan JW, et al. (1997) Hormonal changes and catabolic/anabolic imbalance in chronic heart failure and their importance for cardiac cachexia. Circulation 96: 526–534.
39. Ozcelik C, Erdmann B, Pilz B, Wettschureck N, Britsch S, et al. (2002) Conditional mutation of the ErbB2 (HER2) receptor in cardiomyocytes leads to dilated cardiomyopathy. Proc Natl Acad Sci U S A 99: 8880–8885.
40. Seidman A, Hudis C, Pierri MK, Shak S, Paton V, et al. (2002) Cardiac dysfunction in the trastuzumab clinical trials experience. J Clin Oncol 20: 1215–1221.
41. Perez EA, Rodeheffer R (2004) Clinical cardiac tolerability of trastuzumab. J Clin Oncol 22: 322–329.
42. Redemann N, Holzmann B, von Ruden T, Wagner EF, Schlessinger J, et al. (1992) Anti-oncogenic activity of signalling-defective epidermal growth factor receptor mutants. Mol Cell Biol 12: 491–498.
43. Ikeda K, Tojo K, Tokudome G, Hosoya T, Harada M, et al. (2000) The effects of sarpogrelate on cardiomyocyte hypertrophy. Life Sci 67: 2991–2996.
44. Zou Y, Akazawa H, Qin Y, Sano M, Takano H, et al. (2004) Mechanical stress activates angiotensin II type 1 receptor without the involvement of angiotensin II. Nat Cell Biol 6: 499–506.
45. Matsuura K, Wada H, Nagai T, Iijima Y, Minamino T, et al. (2004) Cardiomyocytes fuse with surrounding noncardiomyocytes and reenter the cell cycle. J Cell Biol 167: 351–363.
46. Honda A, Matsuura K, Fukushima N, Tsurumi Y, Kasanuki H, et al. (2009) Telmisartan induces proliferation of human endothelial progenitor cells via PPARgamma-dependent PI3K/Akt pathway. Atherosclerosis 205: 376–384.
47. Matsuura K, Nagai T, Nishigaki N, Oyama T, Nishi J, et al. (2004) Adult cardiac Sca-1-positive cells differentiate into beating cardiomyocytes. J Biol Chem 279: 11384–11391.

Journal of Cardiology (2012) 59, 14–21

available at www.sciencedirect.com

ScienceDirect

journal homepage: www.elsevier.com/locate/jjcc

Original article

Oral treatment with nicorandil at discharge is associated with reduced mortality after acute myocardial infarction

Yasuhiko Sakata (MD, PhD)[a,*,1], Daisaku Nakatani (MD, PhD)[a,1], Masahiko Shimizu (MD, PhD)[a,1], Shinichiro Suna (MD, PhD)[a,1], Masaya Usami (MD)[a,1], Sen Matsumoto (MD)[a,1], Masahiko Hara (MD)[a,1], Satoru Sumitsuji (MD)[a,b,1], Shigeo Kawano (MD)[c,1], Katsuomi Iwakura (MD)[d,1], Toshimitsu Hamasaki (PhD)[e,1], Hiroshi Sato (MD, PhD, FJCC)[f,1], Shinsuke Nanto (MD, PhD, FJCC)[a,b,1], Masatsugu Hori (MD, PhD, FJCC)[g,1], Issei Komuro (MD, PhD, FJCC)[a,1]

[a] *Department of Cardiovascular Medicine, Osaka University Graduate School of Medicine, Suita, Osaka, Japan*
[b] *Department of Advanced Cardiovascular Therapeutics, Osaka University Graduate School of Medicine, Suita, Osaka, Japan*
[c] *Cardiovascular Division, Kawachi General Hospital, Higashi-osaka, Osaka, Japan*
[d] *Division of Cardiology, Sakurabashi Watanabe Hospital, Osaka, Osaka, Japan*
[e] *Department of Biomedical Statistics, Osaka University Graduate School of Medicine, Suita, Osaka, Japan*
[f] *School of Human Welfare Studies Health Care Center and Clinic, Kwansei Gakuin University, Nishinomiya, Osaka, Japan*
[g] *Osaka Medical Center for Cancer and Cardiovascular Disease, Osaka, Osaka, Japan*

Received 28 May 2011; received in revised form 1 August 2011; accepted 4 August 2011
Available online 15 September 2011

KEYWORDS
Nicorandil;
Acute myocardial infarction;
Mortality;
Secondary prevention

Summary
Background: Previous studies showed that nicorandil can reduce coronary events in patients with coronary artery disease. However, it is unclear whether oral nicorandil treatment may reduce mortality following acute myocardial infarction (AMI).
Methods and Results: We examined the impact of oral nicorandil treatment on cardiovascular events in 1846 AMI patients who were hospitalized within 24 h after AMI onset, treated with emergency percutaneous coronary intervention (PCI), and discharged alive. Patients

* Corresponding author at: Department of Cardiovascular Medicine, Osaka University Graduate School of Medicine, 2-2 Yamadaoka, Suita 565-0871, Japan. Tel.: +81 6 6879 6612; fax: +81 6 6879 6613.
E-mail address: sakatayk@cardiology.med.osaka-u.ac.jp (Y. Sakata).
[1] On Behalf of the Osaka Acute Coronary Insufficiency Study (OACIS) Investigators, see Appendix A.

doi:10.1016/j.jjcc.2011.08.001

were divided into those with (Group N, $n=535$) and without (Group C, $n=1311$) oral nicorandil treatment at discharge. No significant differences in age, gender, body mass index, prevalence of coronary risk factors, or history of myocardial infarction existed between the two groups; however, higher incidences of multi-vessel disease, and a lower rate of successful PCI were observed in Group N. During the median follow-up of 709 (340–1088) days, all-cause mortality rate was 43% lower in Group N compared with Group C (2.4% vs. 4.2%, stratified log-rank test: $p=0.0358$). Multivariate Cox regression analysis revealed that nicorandil treatment was associated with all-cause death after discharge (Hazard ratio 0.495, 95% CI: 0.254–0.966, $p=0.0393$), but not for other cardiovascular events such as re-infarction, admission for heart failure, stroke and arrhythmia. *Conclusions:* The results suggest that oral administration of nicorandil is associated with reduced incidence of death in the setting of secondary prevention after AMI.

Introduction

Although recent progress in the management of acute myocardial infarction (AMI) has decreased mortality [1–3], long-term mortality remains high in post-AMI patients [4]. To further decrease mortality rates in the clinical setting after AMI, numerous efforts have been directed towards the pharmacological modification of left ventricular (LV) performance and remodeling, as well as stabilization of atherosclerotic coronary plaques, as it has been shown to be associated with prognosis [5]. In this context, the anti-anginal drug nicorandil is one of the promising candidates for improving outcomes of post-AMI patients due to its cardioprotective properties [6–19].

Nicorandil is a nicotinamide ester that possesses K-ATP channel-activating and nitrate-like properties and is being increasingly used to treat coronary artery disease (CAD). Nicorandil relieves symptoms of ischemia and also has numerous cardioprotective properties, such as pharmacological preconditioning [6–8], restoration of cardiac blood flow to ischemic and no-reflow myocardium [9–13], prevention of Ca^{2+} overload [14,15], and attenuation of cardiac sympathetic nerve injury [16–18], and so on. However, although the effects of nicorandil in protection of the myocardium during acute ischemic injury have been extensively reported in the clinical setting [9–13,17,20–25], little is known about the long-term impacts of nicorandil on mortality and secondary complications after AMI [18,26].

In the present study, we examined the mortality impact of oral nicorandil at discharge using a relatively large patient cohort in the setting of secondary prevention after AMI.

Methods

The Osaka acute coronary insufficiency study (OACIS)

The Osaka acute coronary insufficiency study (OACIS) is a prospective, multi-center observational study designed to collect and analyze demographic, procedural, outcome data, and blood samples in patients with AMI at 25 collaborating hospitals in the Osaka region of Japan [3,27–30]. As part of the OACIS, research cardiologists and specialized research nurses recorded data on socio-demographic variables, medical histories, therapeutic procedures, and clinical events during patient hospitalization, and also obtained follow-up clinical data at 3, 6, and 12 months after the occurrence of AMI, and annually thereafter. Information was obtained from hospital medical records and by direct interviews with patients, their family members, and their treating physicians. All data were transmitted to the data collection center at the Department of Cardiovascular Medicine, Osaka University Graduate School of Medicine, Suita, Japan for processing and analysis. The diagnosis of AMI required the presence of two of the following three criteria: (1) history of central chest pressure, pain, or tightness lasting more than 30 min, (2) ST-segment elevation 0.1 mV in 1 limb lead or 2 precordial leads, and (3) an increase in serum creatine kinase (CK) concentration of two times the upper limit of normal.

Patients

Among the patients registered with the OACIS registry, 1846 consecutive patients fulfilling the following criteria: (1) admission within 24 h after the onset of AMI between January 2005 and March 2009, (2) treatment with emergency percutaneous coronary intervention (PCI) on admission, and (3) survival discharge, were enrolled in the study. Of these patients, 535 were treated with oral nicorandil at discharge (Group N), while the remaining 1311 patients did not receive nicorandil at discharge (Group C).

Clinical endpoints

The demographic and clinical data and the primary endpoints during the five-year period following discharge, all-cause mortality, non-fatal re-infarction, re-admission for heart failure, and coronary revascularization, including PCI and coronary artery bypass grafting, were compared between patients in Groups N and C.

Statistical analysis

Results are expressed as medians (25th and 75th percentiles) or mean ± SD for continuous variables, and qualitative data are presented as numbers or percentages. Differences of continuous variables between groups were assessed using the Student's *t*-test, whereas categorical variables were compared using the chi-square test. Factors influencing mortality were analyzed using a multivariate Cox proportional hazard regression model with 14 variables from major patient backgrounds and treatments to minimize

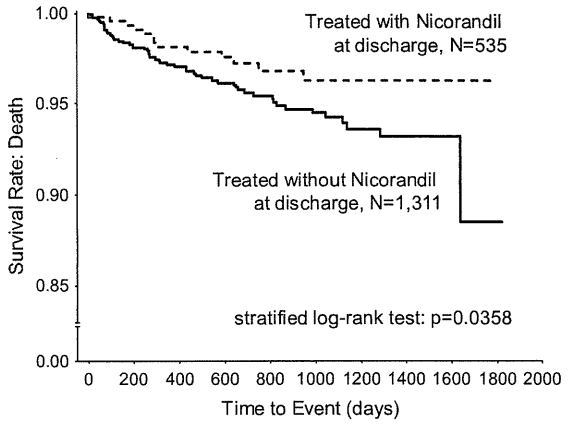

Figure 1 Kaplan–Meier plots for mortality during the five-year follow-up period following discharge for AMI. *p* value after adjustment with variables that had *p* values of <0.1 in the multivariate cox proportional hazard model is <0.05.

the effect of co-founders. Variables included in the model were age, gender, obesity, diabetes, hypertension, dyslipidemia, smoking, multi-vessel disease, PCI success, and prescription of statins, renin angiotensin system inhibitors, or beta-blockers. Survival curves were constructed using the Kaplan–Meier method, and the significance of differences in survival was assessed using the stratified log-rank test with variables as strata suggested by Cox regression. Analysis was performed using SAS version 9.1.3 for Windows (SAS Inc., Cary, NC) and PASW Statistics, version 18.0 (SPSS Inc., Chicago, IL). For all analyses, statistical significance was set at $p < 0.05$.

Results

The study population consisted of 535 patients who received nicorandil at discharge (Group N) and 1311 patients who did not (Group C). The patient baseline characteristics, including the cardiovascular medications being taken before and during the study, are summarized in Table 1. No significant differences in age, gender, body mass index, prevalence of coronary risk factors of diabetes, hypertension, dyslipidemia, obesity and smoking, or history of myocardial infarction were found between the two groups. However, a higher incidence of multi-vessel disease and treatment with intra-aortic balloon pumping, and a lower rate of successful PCI, defined as presence of TIMI3 flow grade after the procedures, were noted in Group N, suggesting that Group N included patients with more severe clinical conditions.

The median follow-up period was 709 (340–1088) days. During the follow-up period, the all-cause mortality rate was 43% lower in Group N compared with Group C, although this difference was not significant (2.4% vs. 4.2%, log-rank test: $p = 0.0849$). However, multivariate Cox proportional hazard analysis revealed that several variables were correlated with mortality following discharge of the AMI patients. After adjustment with the variables, Kaplan–Meier curves for mortality showed a significant difference between Groups N and C (stratified log-rank test: $p = 0.0358$, Fig. 1).

Despite the fact that patients of both groups were also administered other secondary prevention drugs, nicorandil was the only drug to have an association with decreased mortality (Table 2). Multivariate Cox proportional hazard analysis revealed that nicorandil treatment was a predictor for all-cause death after discharge (Hazard ratio (HR) 0.495, 95% CI: 0.254–0.966, $p = 0.039$), but not for re-infarction, admission for heart failure, arrhythmia and stroke (Table 3). Subgroup analysis revealed that no significant interaction were detected between the impact of nicorandil and variables of age, gender, diabetes, hypertension, dyslipidemia, multi-vessel disease, PCI success, and peak CK levels (Table 4), suggesting that nicorandil treatment displayed a significant reduction in mortality regardless of the subgrouping. In addition, subgroup analysis also suggested that nicorandil treatment was particularly associated with reduced mortality for patients with ages of <75 y.o., with hypertension, or of male gender (Table 4).

Discussion

This is the first study suggesting a mortality benefit of nicorandil for post-AMI patients in the clinical setting. In this retrospective analysis with a relatively large-scale AMI cohort, we have demonstrated that AMI patients who received oral nicorandil treatment displayed a reduction in all-cause mortality during a five-year follow-up period. Our results suggest that nicorandil may have the potential to improve survival outcomes in the setting of secondary prevention after AMI.

The most important finding of the present study is that nicorandil treatment was associated with a nearly 50% reduction in all-cause mortality following discharge for AMI (HR 0.495, 95% CI: 0.254–0.966, $p = 0.0393$). This finding also supports the results of a recent large-scale randomized control study, the Impact of Nicorandil in Angina [IONA] study [31], and a retrospective sub-analysis of the Japanese Coronary Artery Disease (JCAD) study [32], which suggested that nicorandil had a beneficial impact on mortality and morbidity in CAD patients. In the IONA study, a 20 mg twice-daily oral nicorandil treatment group ($N = 2565$) displayed a significant reduction in all cardiovascular events over a placebo group ($N = 2561$) [31]. In addition, the nicorandil group had a trend of reduced mortality compared to the placebo group (4.3% vs. 5.0%, respectively; HR 0.85, $p = 0.222$), although the difference was not statistically significant, likely due to the relatively short follow-up period (mean: 1.6 years). The JCAD study is a large multicenter collaborative prospective observational study designed to investigate risk factors, medication use, and outcomes of CAD patients in Japan ($N = 13,812$) [33]. In a retrospective analysis of the JCAD study, Horinaka et al. [32] compared the incidence of cardiovascular events between 2558 nicorandil-treated and 2558 control patients (mean follow-up: 2.7 years) in the JCAD cohort and revealed that death from all causes (primary endpoint) was 35% lower (HR 0.65, $p = 0.0008$) in the nicorandil group. Further, marked reductions in several secondary endpoints, including cardiac death (56%), fatal myocardial infarction (56%), cerebral or vascular death (71%), and congestive heart failure (33%), were noted in the nicorandil group [32]. Taken together, these lines of evidence suggest

Table 1 Patient characteristics of the nicorandil (Group N) and non-nicorandil (Group C) groups.

Variable	Group C ($n=1311$)	Group N ($n=535$)	p Value
Age (years)	65.7 ± 12.1	66.2 ± 11.8	0.388
Male	990 (75.5%)	411 (76.8%)	0.589
Symptom to admission time (h)	5.2 ± 5.5	4.9 ± 5.5	0.255
STEMI	1129 (86.8%)	467 (87.5%)	0.76
Killip class >1	1067 (85.3%)	429 (82.7%)	0.192
Cardiac pulmonary arrest	38 (2.9%)	12 (2.2%)	0.528
Peak creatine kinase (U/L)	2971 ± 2645	3144 ± 2634	0.223
Serum creatinine (mg/dL)	1.04 ± 1.16	1.06 ± 1.19	0.752
Common comorbidities			
Obesity	405 (32.6%)	174 (33.5%)	0.739
Diabetes mellitus	416 (31.7%)	192 (35.9%)	0.091
Hypertension	838 (65.5%)	342 (65.9%)	0.913
Dyslipidemia	557 (44.3%)	250 (48.3%)	0.142
Smoking history	786 (60.9%)	328 (62.4%)	0.595
Previous MI	149 (11.5%)	58 (11.0%)	0.807
Angiographic information			
Initial TIMI grade			0.484
0	754 (57.8%)	304 (57.3%)	
1	142 (10.9%)	54 (10.2%)	
2	246 (18.9%)	93 (17.5%)	
3	163 (12.5%)	80 (15.1%)	
Multiple vessel disease	534 (41.0%)	269 (50.5%)	
Collateral vessels	402 (31.2%)	164 (31.5%)	
Infarct related artery: LAD	552 (41.8%)	242 (46.0%)	
Reperfusion therapy			
PCI	1331 (100%)	535 (100%)	1
Stent	1225 (93.5%)	507 (94.9%)	0.282
Thrombectomy	921 (70.3%)	354 (66.2%)	0.086
Drug-eluting stent	89 (6.8%)	35 (6.8%)	0.918
PCPS	29 (2.2%)	6 (1.1%)	0.135
IABP	184 (14.0%)	97 (18.1%)	0.032
Emergent CABG	9 (0.7%)	5 (0.9%)	0.563
Temporary pacing	275 (21.3%)	101 (19.3%)	0.371
Successful reperfusion	1217 (93.6%)	481 (91.1%)	0.07
No-reflow phenomenon	36 (5.5%)	16 (6.8%)	0.517
Medications at discharge			
Anti-platelets	1289 (98.3%)	529 (98.9%)	0.529
ACEIs	419 (32.0%)	279 (52.1%)	<0.001
ARBs	647 (49.4%)	175 (32.7%)	<0.001
ACEI and/or ARB	1038 (79.2%)	435 (81.3%)	0.038
β-Blockers	813 (62.0%)	303 (56.6%)	0.036
Statin	689 (52.6%)	298 (55.7%)	0.237
Ca channel blockers	205 (15.6%)	70 (13.1%)	0.171
Nitrates	255 (19.5%)	91 (17.0%)	0.237
Diuretics	336 (25.6%)	143 (26.7%)	0.64

Results are expressed as mean ± SD for continuous variables. ACEI, angiotensin converting enzyme inhibitor; ARB, angiotensin II receptor blocker; CABG, coronary artery bypass graft; IABP, intraaortic balloon pumping; MI, myocardial infarction; PCI, percutaneous coronary intervention; PCPS, percutaneous cardio-pulmonary support; STEMI, ST elevation myocardial infarction; TIMI, thrombolysis in myocardial infarction.

that nicorandil has a beneficial effect for reducing mortality in patients with CAD, including post-AMI patients.

It is noteworthy that nicorandil treatment at discharge was associated with mortality reduction (Table 1), although nicorandil had been likely used as an adjunct to other cardioprotective drugs, rather than as an alternative, which is supported by the comparable prevalence of secondary prevention drugs between Groups N and C. Accordingly, nicorandil is potentially a good candidate to be given in an additive manner with popular cardiovascular secondary

Table 2 Predictors for death after discharge.

Variable	Multivariate cox proportional hazard model			
	HR	Lower limit	Upper limit	*p* Value
Statins	0.904	0.516	1.583	0.7247
RAS inhibitors	0.894	0.488	1.638	0.7166
Beta blockers	1.408	0.802	2.470	0.2332
Ca channel blockers	0.493	0.221	1.102	0.0849
Nicorandil	0.495	0.254	0.966	0.0393

Variables: age, gender, diabetes mellitus, hypertension, dyslipidemia, smoking, multi-vessel disease, successful percutaneous coronary, intervention, peak creatine kinase level, beta-blockers, renin-, angiotensin inhibitors, statins, calcium channel blockers, and nicorandil.

Table 3 Impact of oral nicorandil on cardiac events.

Cardiovascular event	HR	95% CI	*p* Value
Death	0.495	(0.254–0.966)	0.039
Myocardial infarction	0.873	(0.469–1.624)	0.667
Admission for heart failure	0.741	(0.410–1.338)	0.319
Arrhythmia	0.737	(0.360–1.509)	0.366
Stroke	0.363	(0.107–1.229)	0.103

Variables: age, gender, diabetes mellitus, hypertension, dyslipidemia, smoking, multi-vessel disease, successful percutaneous coronary, intervention, peak creatine kinase level, beta-blockers, renin-, angiotensin inhibitors, statins, calcium channel blockers, and nicorandil.

Table 4 Predictors for death after discharge.

Subgroup		*N*	HR	95% CI	*p* Value	*p* for Interaction
Age (years)	<75	1242	0.294	(0.088–0.984)	0.0471	0.2012
	≥75	435	0.817	(0.371–1.797)	0.6145	
Gender	Female	431	0.792	(0.219–2.866)	0.7224	0.4888
	Male	1394	0.474	(0.227–0.991)	0.0472	
Diabetes mellitus	No	1210	0.481	(0.182–1.269)	0.1391	0.6086
	Yes	608	0.610	(0.259–1.438)	0.2587	
Hypertension	No	618	0.802	(0.215–2.990)	0.7425	0.1672
	Yes	1180	0.429	(0.200–0.921)	0.0298	
Dyslipidemia	No	954	0.542	(0.250–1.173)	0.1199	0.6556
	Yes	805	0.308	(0.082–1.152)	0.0802	
Multi-vessel disease	No	1006	0.596	(0.205–1.733)	0.3423	0.8772
	Yes	803	0.483	(0.213–1.096)	0.0815	
PCI success	No	130	0.365	(0.041–3.291)	0.3692	0.9888
	Yes	1647	0.544	(0.277–1.069)	0.0775	
Peak CK level (U/L)	<3000	1203	0.532	(0.227–1.247)	0.1464	0.7414
	≥3000	621	0.530	(0.198–1.418)	0.2061	

CK, creatine kinase; PCI, percutaneous coronary intervention.

prevention drugs, such as beta-blockers and/or rennin-angiotensin system inhibitors. It is also noteworthy that the present study suggested that nicorandil was beneficial for all patients in the secondary prevention settings after AMI, because no significant interaction were detected after subgroup analysis (Table 4). In addition, the mortality benefit of nicorandil seemed particularly apparent for patients with ages <75 y.o., with hypertension, and of male gender (Table 4). Notably, a 71% reduction in mortality rate was found in nicorandil-treated patients with ages <75 y.o. (HR 0.294, 95% CI: 0.088–0.984, $p = 0.047$). Therefore, we suggest that nicorandil may represent a potent first-line drug for all patients after AMI, particularly for those with ages <75 y.o., male gender, or hypertension.

Although details of the mechanisms are unclear, the following pharmacologic and other properties of nicorandil may explain why this drug improves survival in patients with CAD or AMI. First, cardioprotective effects exerted by nicorandil during the acute stage of AMI and/or acute myocardial ischemia [9–13,17,20–25] may have also provided benefits in the convalescent or chronic stages of AMI. Second, as suggested in the J-WIND study [26], nicorandil treatment during the chronic phase of AMI may have improved left ventricular function, resulting in a reduction of mortality. Third, the positive effects of nicorandil on sympathetic nerve activity might have played a role in improving survival. Indeed, although it was a small sample-size study from a single center, Kasama et al. [18] reported that the long-term (six months) administration of 15 mg/dL nicorandil resulted in improved cardiac sympathetic nerve activity in AMI patients. Fourth, the anti-hypertensive properties of nicorandil might have reduced long-term mortality [34]. As discussed previously, nicorandil appeared to have been prescribed in an additive manner in the present cohort, rather than as an alternative to the other administered cardioprotective or antihypertensive drugs. Accordingly, the adjunctive use of nicorandil may have lowered blood pressure more effectively than in the control group, resulting in a reduction in long-term mortality. Finally, better long-term compliance and lack of tolerance to nicorandil [35] might be associated with improved mortality.

In the present study, we did not observe significant reductions in other cardiac events in Group N patients, unlike the results from the IONA study [31] and JCAD sub-study [32]. This discrepancy may have been due to differences in the backgrounds of the study populations; we only included patients who survived AMI in the present study, whereas the other two studies included individuals with stable angina or CAD [31,32]. Accordingly, it appears that the study cohort might have been more strictly treated with secondary prevention medications in the present study, as the prevalence of co-administered cardioprotective drugs such as antiplatelets, ACE inhibitors, angiotensin II receptor blockers (ARBs), β-blockers, and statin was higher than or at least equal to those in the IONA and JCAD studies [31,32]. In addition, the cohort subjects in the present study had all received emergent PCI for infarct related arteries and were likely to have undergone subsequent PCI for other diseased coronary arteries in the acute or convalescent stage of AMI, possibly resulting in a reduction of residual myocardial ischemia and prevention of ischemia-related cardiovascular complications. Therefore, the beneficial effects of nicorandil on cardiovascular events other than mortality may have been masked by the increased usage of co-administered cardioprotective drugs, as well as differences in the management of diseased coronary arteries.

A few limitations of the study warrant mention. First, as this was a retrospective observational study, precise information concerning the dose, duration and patient compliance for nicorandil treatment, was not available. In addition, information about cardiac function at discharge was not obtained in the present study. Second, as it was also observed that patients in Group N appeared to have more severe clinical CAD conditions, including a higher incidence of multi-vessel disease and a lower rate of successful PCI, the overall efficacy of nicorandil may have been underestimated. Third, the present study enrolled only the subjects who underwent emergent PCI in the acute stage of AMI. Accordingly, caution may be needed when interpreting the results for AMI patients who did not receive emergent PCI. Fourth, although the results suggested that nicorandil was effective to reduce mortality in those with age of <75 y.o. or those with male gender, the mechanisms were unclear and thus remain to be disclosed.

In conclusion, we have demonstrated that the oral administration of nicorandil following AMI was associated with reduced incidence of death for all patients, particularly in individuals with ages <75 y.o., male gender and hypertension. Although further randomized clinical investigations are needed, the promising clinical outcomes presented here suggest that nicorandil on oral administration may be effective for treating CAD and is expected to improve patient survival in the secondary prevention setting following AMI.

Acknowledgments

We express our sincere appreciation to Mariko Kishida, Rie Nagai, Nanase Muraoka, Hiroko Takemori, Akiko Yamagishi, Kumiko Miyoshi, Chizuru Hamaguchi, Hiroko Machida, Mariko Yoneda, Nagisa Yoshioka, Mayuko Tomatsu, Kyoko Tatsumi, Tomoko Mizuoka, Shigemi Kohara, Junko Tsugawa, Junko Isotani, and all other OACIS research coordinators and nurses for their excellent assistance with data collection.

Appendix A. OACIS investigators

Chair: Issei Komuro, Department of Cardiovascular Medicine, Osaka University Graduate School of Medicine, 2-2 Yamada-oka, Suita 565-0871, Japan

Secretariats: Yasuhiko Sakata (Chief), Daisaku Nakatani, Shinichiro Suna, Masaya Usami, Sen Matsumoto, Masahiko Hara, Mariko Kishida, Rie Nagai: Department of Cardiovascular Medicine, Osaka University Graduate School of Medicine, Suita, Japan

Investigators (institutions in alphabetical order): Yoshiyuki Kijima, Yusuke Nakagawa, Minoru Ichikawa, Higashi-Osaka City General Hospital, Higashi-Osaka, Japan; Young-Jae Lim, Shigeo Kawano, Kawachi General Hospital, Higashi-Osaka, Japan; Hiroshi Sato, Kwasnsei Gakuin University, Nishinomiya, Japan; Takashi Shimazu, Hisakazu Fuji, Kazuhiro Aoki, Kobe Ekisaikai Hospital, Kobe, Japan; Seiki Nagata, Yoshio Ishida, Masaaki Uematsu, Tetsuya Watanabe, Masashi Fujita, Masaki Awata, Kansai Rosai Hospital, Amagasaki, Japan; Michio Sugii, Meiwa Hospital, Nishinomiya, Japan; Masatake Fukunami, Takahisa Yamada, Takashi Morita, Osaka General Medical Center, Osaka, Japan; Shinji Hasegawa, Nobuyuki Ogasawara, Osaka Kosei Nenkin Hospital, Osaka, Japan; Tatsuya Sasaki, Yoshinori Yasuoka, Osaka Minami Medical Center, National Hospital Organization, Kawachinagano, Japan; Hideo Kusuoka, Yukihiro Koretsune, Yoshio Yasumura Y, Keiji Hirooka, Osaka Medical Center, National Hospital Organization, Osaka, Japan; Masatsugu Hori (previous Chair), Osaka Prefectural Hospital Organization Osaka Medical Center for Cancer and Cardiovascular Diseases; Kazuhisa Kodama, Yasunori Ueda, Kazunori Kashiwase, Akio Hirata, Mayu

Nishio, Mitsutoshi Asai, Osaka Police Hospital, Osaka, Japan; Yoshio Yamada, Jun Tanouchi, Masami Nishino, Hiroyasu Kato, Ryu Shutta, Osaka Rosai Hospital, Sakai, Japan; Shintaro Beppu, Akio Kohama, Hiroyoshi Yamamoto, Osaka Seamens Insurance Hospital, Osaka, Japan; Issei Komuro, Shinsuke Nanto, Kinya Otsu, Yasushi Matsumura, Kazuhiro Yamamoto, Tetsuo Minamino, Satoru Sumitsuji, Yasuhiko Sakata, Shungo Hikoso, Daisaku Nakatani, Osaka University Graduate School of Medicine, Suita, Japan; Toru Hayashi, Yasuji Doi, Ken-ichiro Okada, Noritoshi Ito, Saiseikai Senri Hospital, Suita, Japan; Kenshi Fujii, Katsuomi Iwakura, Atsushi Okamura, Motoo Date, Yoshiharu Higuchi, Sakurabashi Watanabe Hospital, Osaka, Japan; Noriyuki Akehi, Settsu Iseikai Hospital, Settsu, Japan; Eiji Hishida, Teramoto Memorial Hospital, Kawachinagano, Japan; and Shiro Hoshida, Kazuhiko Hashimura, Takayoshi Adachi, Yao Municipal Hospital, Yao, Japan.

References

[1] Keith AAF, Philippe GS, Kim AE, Shaun GG, Frederick Jr AA, Christopher BG, Marcus DF, Andrzej B, Ann Q, Joel MG, GRACE Investigators. Decline in rates of death and heart failure in acute coronary syndromes, 1999–2006. JAMA 2007;297:1892–900.

[2] Nakamura M, Yamashita T, Yajima J, Oikawa Y, Ogasawara K, Sagara K, Kirigaya H, Koike A, Nagashima K, Ohtsuka T, Uejima T, Suzuki S, Sawada H, Aizawa T. Clinical outcome after acute coronary syndrome in Japanese patients: an observational cohort study. J Cardiol 2010;55(1):69–76.

[3] Usami M, Sakata Y, Nakatani D, Shimizu M, Suna S, Matsumoto S, Hori M, Sato H, Osaka Acute Coronary Insufficiency Study (OACIS) Group. Effect of intracoronary thrombectomy on 30-day mortality in non-diabetic patients with acute hyperglycemia after acute myocardial infarction. J Cardiol 2009;53(3):429–36.

[4] Jernberg T, Johanson P, Held C, Svennblad B, Lindbäck J, Wallentin L, SWEDEHEART/RIKS-HIA. Association between adoption of evidence-based treatment and survival for patients with ST-elevation myocardial infarction. JAMA 2011;305(16):1677–84.

[5] Burns RJ, Gibbons RJ, Yi Q, et al. The relationships of left ventricular ejection fraction, end-systolic volume index and infarct size to six-month mortality after hospital discharge following acute myocardial infarction treated by thrombolysis. J Am Coll Cardiol 2002;39:30–6.

[6] Menasché P, Kevelaitis E, Mouas C, Grousset C, Piwnica A, Bloch G. Preconditioning with potassium channel openers. A new concept for enhancing cardioplegic protection? J Thorac Cardiovasc Surg 1995;110(6):1606–13.

[7] Sugimoto S, Iwashiro K, Monti F, Dawodu AA, Schiariti M, Puddu PE. The risk of myocardial stunning is decreased concentration-dependently by KATP channel activation with nicorandil before high K^+ cardioplegia. Int J Cardiol 1995;48(1):11–25.

[8] Imagawa J, Baxter GF, Yellon DM. Myocardial protection afforded by nicorandil and ischaemic preconditioning in a rabbit infarct model in vivo. J Cardiovasc Pharmacol 1998;31(1):74–9.

[9] Ito H, Taniyama Y, Iwakura K, Nishikawa N, Masuyama T, Kuzuya T, et al. Intravenous nicorandil can preserve microvascular integrity and myocardial viability in patients with reperfused anterior wall myocardial infarction. J Am Coll Cardiol 1999;33:654–60.

[10] Sakata Y, Kodama K, Komamura K, Lim YJ, Ishikura F, Hirayama A, Kitakaze M, Masuyama T, Hori M. Salutary effect of adjunctive intracoronary nicorandil administration on restoration of myocardial blood flow and functional improvement in patients with acute myocardial infarction. Am Heart J 1997;133(6):616–21.

[11] Sakata Y, Kodama K, Ishikura F, Komamura K, Hasegawa S, Sakata Y, Hirayama A. Disappearance of the 'no-reflow' phenomenon after adjunctive intracoronary administration of nicorandil in a patient with acute myocardial infarction. Jpn Circ J 1997;61(5):455–8.

[12] Sakata Y, Kitakaze M, Kuzuya T, Hirayama A, Kodama K, Hori M. Beneficial effects of nicorandil, a K^+-ATP channel opener, on the "no-reflow" myocardium. Ther Res 1999;20(4):934–8 (Japanese).

[13] Ito N, Nanto S, Doi Y, Sawano H, Masuda D, Yamashita S, Okada K, Kaibe S, Hayashi Y, Kai T, Hayashi T. High index of microcirculatory resistance level after successful primary percutaneous coronary intervention can be improved by intracoronary administration of nicorandil. Circ J 2010;74(5):909–15.

[14] Ishida H, Higashijima N, Hirota Y, Genka C, Nakazawa H, Nakaya H, Sato T. Nicorandil attenuates the mitochondrial Ca^{2+} overload with accompanying depolarization of the mitochondrial membrane in the heart. Naunyn Schmiedebergs Arch Pharmacol 2004;369(2):192–7.

[15] Lopez JR, Jahangir R, Jahangir A, Shen WK, Terzic A. Potassium channel openers prevent potassium-induced calcium loading of cardiac cells: possible implications in cardioplegia. J Thorac Cardiovasc Surg 1996;112:820–31.

[16] Miura T, Kawamura S, Tatsuno H, et al. Ischemic preconditioning attenuates cardiac sympathetic nerve injury via ATP-sensitive potassium channels during myocardial ischemia. Circulation 2001;104:1053–8.

[17] Kasama S, Toyama T, Kumakura H, et al. Effects of nicorandil on cardiac sympathetic nerve activity after reperfusion therapy in patients with first anterior acute myocardial infarction. Eur J Nucl Med Mol Imaging 2005;32:322–8.

[18] Kasama S, Toyama T, Sumino H, Kumakura H, Takayama Y, Ichikawa S, et al. Long-term nicorandil therapy improves cardiac sympathetic nerve activity after reperfusion therapy in patients with first acute myocardial infarction. J Nucl Med 2007;48:1676–82.

[19] Iwakura K, Ito H, Okamura A, Koyama Y, Date M, Higuchi Y, Inoue K, Kimura R, Nagai H, Imai M, Toyoshima Y, Ozawa M, Ito N, Okazaki Y, Shibuya M, Suenaga H, Kubota A, Fujii K. Nicorandil treatment in patients with acute myocardial infarction: a meta-analysis. Circ J 2009;73(5):925–31.

[20] Fukuzawa S, Ozawa S, Inagaki M, Shimada K, Sugioka J, Tateno K, et al. Nicorandil affords cardioprotection in patients with acute myocardial infarction treated with primary percutaneous transluminal coronary angioplasty: assessment with thallium-201/iodine-123 BMIPP dual SPECT. J Nucl Cardiol 2000;7:447–53.

[21] Ota S, Nishikawa H, Takeuchi M, Nakajima K, Nakamura T, Okamoto S, et al. Impact of nicorandil to prevent reperfusion injury in patients with acute myocardial infarction: sigmart multicenter angioplasty revascularization trial (SMART). Circ J 2006;70:1099–104.

[22] Ueda H, Nakayama Y, Tsumura K, Yoshimaru K, Hayashi T, Yoshikawa J. Intravenous nicorandil can reduce the occurrence of ventricular fibrillation and QT dispersion in patients with successful coronary angioplasty in acute myocardial infarction. Can J Cardiol 2004;20:625–9.

[23] Kobayashi Y, Goto Y, Daikoku S, Itoh A, Miyazaki S, Ohshima S, et al. Cardioprotective effect of intravenous nicorandil in patients with successful reperfusion for acute myocardial infarction. Jpn Circ J 1998;62:183–9.

[24] Sugimoto K, Ito H, Iwakura K, Ikushima M, Kato A, Kimura R, et al. Intravenous nicorandil in conjunction with coronary reperfusion therapy is associated with better clinical and

functional outcomes in patients with acute myocardial infarction. Circ J 2003;67:295–300.
[25] Ishii H, Ichimiya S, Kanashiro M, Amano T, Imai K, Murohara T, et al. Impact of a single intravenous administration of nicorandil before reperfusion in patients with ST-segment-elevation myocardial infarction. Circulation 2005;112: 1284–8.
[26] Kitakaze M, Asakura M, Kim J, Shintani Y, Asanuma H, Hamasaki T, et al.; J-WIND Investigators. Human atrial natriuretic peptide and nicorandil as adjuncts to reperfusion treatment for acute myocardial infarction (J-WIND): two randomised trials. Lancet 2007;370(9597):1483–93. Erratum in: Lancet 2008;370(9605):2102.
[27] Kinjo K, Sato H, Ohnishi Y, Hishida E, Nakatani D, Mizuno H, Imai K, Nanto S, Naka M, Matsumura Y, et al. Impact of high-sensitivity C-reactive protein on predicting long-term mortality of acute myocardial infarction. Am J Cardiol 2003;91: 931–5.
[28] Kinjo K, Sato H, Sato H, Ohnishi Y, Hishida E, Nakatani D, Mizuno H, Fukunami M, Koretsune Y, Takeda H, Hori M. Prognostic significance of atrial fibrillation/atrial flutter in patients with acute myocardial infarction treated with percutaneous coronary intervention. Am J Cardiol 2003;92: 1150–4.
[29] Kurotobi T, Sato H, Kinjo K, et al., OACIS Group. Reduced collateral circulation to the infarct-related artery in elderly patients with acute myocardial infarction. J Am Coll Cardiol 2004;44:28–34.
[30] Nakatani D, Sato H, Sakata Y, et al. Effect of intracoronary thrombectomy on 30-day mortality in patients with acute myocardial infarction. Am J Cardiol 2007;100:1212–7.
[31] IONA Study Group. Effect of nicorandil on coronary events in patients with stable angina: the impact of nicorandil in angina (IONA) randomized trial. Lancet 2002;359:1269–75.
[32] Horinaka S, Yabe A, Yagi H, Ishimitsu T, Yamazaki T, JCAD Study Investigators, et al. Effects of nicorandil on cardiovascular events in patients with coronary artery disease in the Japanese coronary artery disease (JCAD) study. Circ J 2010;74:503–9.
[33] The Japanese Coronary Artery Disease (JCAD) Study Investigators. Current status of the background of patients with coronary artery disease in Japan: the Japanese coronary artery disease study (The JCAD Study). Circ J 2006;70:1256–62.
[34] Coltart DJ, Coltart DJ, Signy M. Acute hemodynamic effects of single-dose nicorandil in coronary artery disease. Am J Cardiol 1989;63(21):34J–9J.
[35] Krumenacker M, Roland E. Clinical profile of nicorandil: an overview of its hemodynamic properties and therapeutic efficacy. J Cardiovasc Pharmacol 1992;20:S93–102.

Whole-exome sequencing of human pancreatic cancers and characterization of genomic instability caused by *MLH1* haploinsufficiency and complete deficiency

Linghua Wang,[1] Shuichi Tsutsumi,[1] Tokuichi Kawaguchi,[2] Koichi Nagasaki,[3] Kenji Tatsuno,[1] Shogo Yamamoto,[1] Fei Sang,[1] Kohtaro Sonoda,[1] Minoru Sugawara,[3] Akio Saiura,[4] Seiko Hirono,[5] Hiroki Yamaue,[5] Yoshio Miki,[3,6] Minoru Isomura,[3] Yasushi Totoki,[7] Genta Nagae,[1] Takayuki Isagawa,[1] Hiroki Ueda,[1] Satsuki Murayama-Hosokawa,[8] Tatsuhiro Shibata,[7] Hiromi Sakamoto,[9] Yae Kanai,[10] Atsushi Kaneda,[1] Tetsuo Noda,[3] and Hiroyuki Aburatani[1,11]

[1] *Genome Science Division, Research Center for Advanced Science and Technology (RCAST), The University of Tokyo, Tokyo 153-8904, Japan;* [2] *Department of Cell Biology, Cancer Institute, Japanese Foundation for Cancer Research (JFCR), Tokyo 135-8550, Japan;* [3] *Genome Center, Cancer Institute, Japanese Foundation for Cancer Research (JFCR), Tokyo 135-8550, Japan;* [4] *Department of Gastroenterological Surgery, Cancer Institute Hospital, Japanese Foundation for Cancer Research (JFCR), Tokyo 135-8550, Japan;* [5] *Second Department of Surgery, Wakayama Medical University School of Medicine, Wakayama 641-8510, Japan;* [6] *Department of Molecular Genetics, Medical Research Institute, Tokyo Medical and Dental University, Tokyo 113-8510, Japan;* [7] *Division of Cancer Genomics, National Cancer Center Research Institute, Tokyo 104-0045, Japan;* [8] *Department of Obstetrics and Gynecology, Faculty of Medicine, The University of Tokyo, Tokyo 113-8655, Japan;* [9] *Division of Genetics, National Cancer Center Research Institute, Tokyo 104-0045, Japan;* [10] *Division of Molecular Pathology, National Cancer Center Research Institute, Tokyo 104-0045, Japan*

Whole-exome sequencing (Exome-seq) has been successfully applied in several recent studies. We here sequenced the exomes of 15 pancreatic tumor cell lines and their matched normal samples. We captured 162,073 exons of 16,954 genes and sequenced the targeted regions to a mean coverage of 56-fold. This study identified a total of 1517 somatic mutations and validated 934 mutations by transcriptome sequencing. We detected recurrent mutations in 56 genes. Among them, 41 have not been described. The mutation rates varied widely among cell lines. The diversity of the mutation rates was significantly correlated with the distinct *MLH1* copy-number status. Exome-seq revealed intensive genomic instability in a cell line with *MLH1* homozygous deletion, indicated by a dramatically elevated rate of somatic substitutions, small insertions/deletions (indels), as well as indels in microsatellites. Notably, we found that *MLH1* expression was decreased by nearly half in cell lines with an allelic loss of *MLH1*. While these cell lines were negative in conventional microsatellite instability assay, they showed a 10.5-fold increase in the rate of somatic indels, e.g., truncating indels in *TP53* and *TGFBR2*, indicating *MLH1* haploinsufficiency in the correction of DNA indel errors. We further analyzed the exomes of 15 renal cell carcinomas and confirmed *MLH1* haploinsufficiency. We observed a much higher rate of indel mutations in the affected cases and identified recurrent truncating indels in several cancer genes such as *VHL*, *PBRM1*, and *JARID1C*. Together, our data suggest that *MLH1* hemizygous deletion, through increasing the rate of indel mutations, could drive the development and progression of sporadic cancers.

[Supplemental material is available for this article.]

The current understanding of cancer is that it arises as a result of the accumulation of genetic and epigenetic mutations that confer a selective advantage to the cells in which they occur (Vogelstein and Kinzler 2004; Greenman et al. 2007; Stratton et al. 2009). Over the past quarter of a century, many efforts have been made to learn about the causative mutations that drive various types of cancer, including pancreatic cancer, one of the most lethal forms of human cancer. By using the Sanger sequencing method, i.e., PCR amplification followed by plasmid subcloning and DNA sequencing, previous studies have identified thousands of genetic alterations in the cancer genome and provided important insights into the pancreatic cancer biology (Jones et al. 2008; Maitra and Hruban 2008). However, because Sanger sequencing is performed on single amplicons, its throughput is limited, and large-scale sequencing projects are expensive and laborious (Schuster 2008; Metzker 2010). Moreover, it has been reported that it has a limited sensitivity to recognize the mutant DNA allele if it is present in a minor population of cancer cells (Nakahori et al. 1995; Thomas et al. 2006; Qiu et al. 2008). In addition, the bacterial cloning workflows tend to be complex and time-consuming, and bias can be introduced into this step (Thomas et al. 2006).

The advent of next-generation sequencing (NGS) technologies has brought a high level of efficiency to genome sequencing (Schuster 2008; Metzker 2010). The enriched DNA is sequenced directly, avoiding the cloning step (Ng et al. 2009). While whole-genome

[11] **Corresponding author.**
E-mail haburata-tky@umin.ac.jp.
Article published online before print. Article, supplemental material, and publication date are at http://www.genome.org/cgi/doi/10.1101/gr.123109.111.

22:208–219 © 2012 by Cold Spring Harbor Laboratory Press; ISSN 1088-9051/12; www.genome.org

sequencing is the most complete, it remains sufficiently expensive that cost-effective alternatives are important. Target-enrichment strategies allow the selective capture of the genomic regions of interest. Whole-exome sequencing (Exome-seq) through integrating two systems has enabled us to concentrate our sequencing efforts on the protein-coding exons in the human genome. This approach is substantially cost- and labor-efficient (Schuster 2008; Metzker 2010; Biesecker et al. 2011). Moreover, by taking advantage of deep coverage of target regions, it shows an excellent sensitivity for the detection of variants with a minor allele frequency down to 2% (Li et al. 2010). Recent studies have successfully applied Exome-seq to identify genetic changes involved in Mendelian diseases (Choi et al. 2009; Ng et al. 2010). In addition to Exome-seq, full-length transcriptome sequencing (mRNA-seq) offers a fast and inexpensive alternative. It is an easier method to identify coding sequences and capture variants in genes that are expressed, as well as to generate additional information, such as gene expression level and splicing patterns (Sugarbaker et al. 2008; Cirulli et al. 2010).

Genomic instability is a characteristic feature of almost all human cancers (Lengauer et al. 1998; Negrini et al. 2010). Its molecular basis is well understood in hereditary cancers, in which it has been linked to mutations in DNA mismatch repair (MMR) genes. One of the best-documented examples is the hereditary nonpolyposis colon cancer (HNPCC). In general, MMR defects are the result of a germline mutation in one of the MMR genes followed by a hit on the second allele of that gene, or methylation of the promoter of a MMR gene, usually *MLH1*, resulting in the loss of protein function (Fishel et al. 1993; Hemminki et al. 1994). In contrast, the molecular basis of genomic instability in sporadic cancers remains unclear (Negrini et al. 2010).

In the past few years, by use of Sanger sequencing, several consortia have scanned the coding sequences of 18,191–20,661 genes in carcinomas of the colon, breast, and pancreas and in glioblastomas (Sjoblom et al. 2006; Wood et al. 2007; Jones et al. 2008; Parsons et al. 2008). These genome-wide studies reported that mutations targeting caretaker genes (DNA repair genes and mitotic checkpoint genes) were infrequent. To date, no statistical correlation has been described in sporadic cancers between the allelic loss of a caretaker gene and the increased rate of genomic instability. It has been thought that a single copy of the wild-type allele of a caretaker gene is sufficient to perform its normal function, and both alleles of the gene would have to be inactivated before the genome becomes unstable (Bodmer et al. 2008; Negrini et al. 2010). Since the occurrence of two independent somatic mutations at both alleles of the same gene is likely to represent a very rare event (Bodmer et al. 2008), these studies argued that mutations in caretaker genes probably do not account for the presence of genomic instability in many sporadic cancers (Negrini et al. 2010).

We here performed Exome-seq on 15 pancreatic ductal adenocarcinoma (PDAC)–derived cell lines. This study identified 1517 somatic mutations and validated 934 of them by mRNA-seq. We notably found a significant correlation between *MLH1* allelic loss and the increased rate of somatic indel mutations, and we further confirmed this finding in primary renal cell carcinomas (RCCs). In the affected cases, we detected recurrent truncating indels that inactivate tumor suppressor genes, such as *TP53*, *TGFBR2*, and *VHL*. We also observed a higher prevalence of indels in the coding microsatellite sequences. Our data, therefore, indicate that deletion of one copy of the *MLH1* gene results in haploinsufficiency in the correction of DNA indel errors and could be a driving force in pancreatic and renal carcinogenesis.

Results

The performance of Exome-seq

We sequenced the exomes of 15 PDAC-derived cell lines and their matched normal samples (Table 1). On average, 6.6 Gb of high-quality sequence data (about 44.2 million paired 75-base reads) were generated per sample. More than 88% of the sequence reads were uniquely aligned to the human reference genome with the expected insert size and correct orientations, and 68.4% of them fell within the targeted regions (Fig. 1A; Supplemental Fig. S1). The average fold-coverage of each exome was 56× (Supplemental Fig. S2). On average per exome, 96.9% of targeted bases were covered by at least one read, and 83.4% of targeted bases were covered by at least 10 reads (Fig. 1B; Supplemental Fig. S3).

An overview of somatic mutations

By using Exome-seq, we identified a total of 1517 somatic mutations, including 39 nonsense, 833 missense, 423 synonymous substitutions, and 49 substitutions in untranslated regions (UTRs), 137 frame-shift indels and 36 in-frame indels (Fig. 1C). The complete list

Table 1. Characteristics of pancreatic tumor cell lines

Sample OID	Carcinoma type	Pathology	Differentiation	Lymph node metastasis	Tissue derivation	Sample type	*MLH1* status
PA018	Ductal adenocarcinoma	Tubular	Moderately	–	Primary pancreatic tumor	Cell line	LOH
PA028	Ductal adenocarcinoma	Tubular	Moderately	+	Primary pancreatic tumor	Cell line	ROH
PA055	Ductal adenocarcinoma	Tubular	Moderately	+	Primary pancreatic tumor	Cell line	LOH
PA086	Ductal adenocarcinoma	Tubular	Moderately	+	Primary pancreatic tumor	Cell line	ROH
PA090	Ductal adenocarcinoma	Tubular	Well	+	Primary pancreatic tumor	Cell line	ROH
PA107	Ductal adenocarcinoma	Invasive	Moderately to well	–	Primary pancreatic tumor	Cell line	ROH
PA122	Ductal adenocarcinoma	Invasive	Moderately to poorly	–	Primary pancreatic tumor	Cell line	ROH
PA167	Ductal adenocarcinoma	Invasive	Moderately	+	Primary pancreatic tumor	Cell line	LOH
PA182	Ductal adenocarcinoma	Invasive	Moderately	+	Primary pancreatic tumor	Cell line	ROH
PA195	Ductal adenocarcinoma	Tubular	Moderately	+	Primary pancreatic tumor	Cell line	ROH
PA202	Ductal adenocarcinoma	Tubular	Moderately	+	Primary pancreatic tumor	Cell line	LOH
PA215	Ductal adenocarcinoma	Tubular	Poorly	+	Primary pancreatic tumor	Cell line	ROH
PA254	Ductal adenocarcinoma	Tubular	Moderately	–	Primary pancreatic tumor	Cell line	ROH
PA285	Ductal adenocarcinoma	Invasive	Moderately	–	Primary pancreatic tumor	Cell line	HD
PA333	Ductal adenocarcinoma	Tubular	Well	+	Primary pancreatic tumor	Cell line	ROH

ROH indicates retention of heterozygosity; LOH, loss of heterozygosity; and HD, homozygous deletion.

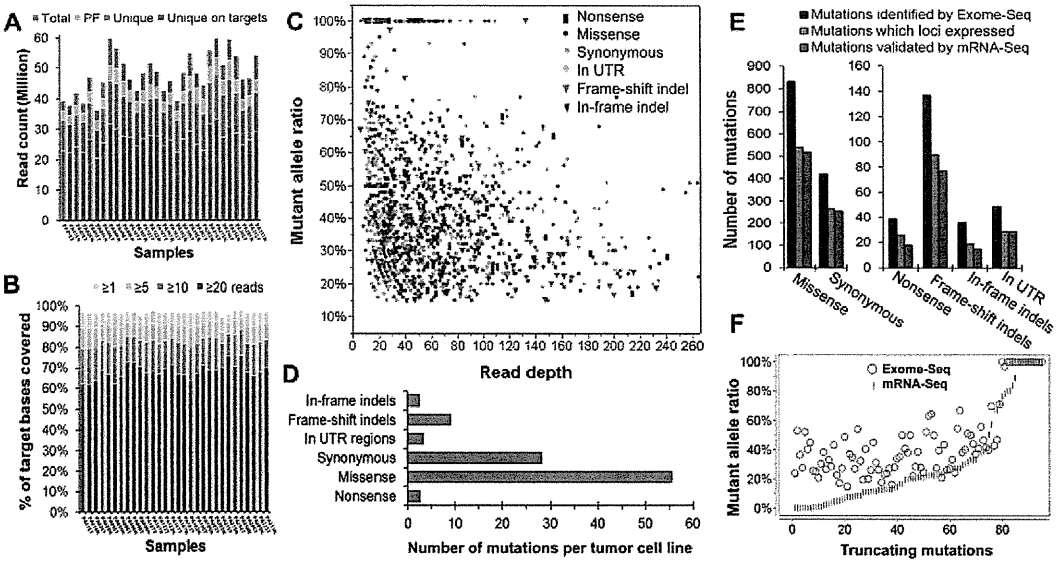

Figure 1. The performance of Exome-seq and a summary of somatic mutations. (*A*) The summary of Exome-seq data. For each sample, the number of raw sequence reads (total), passing filter reads (PF), unique reads that mapped in consistent read pairs (unique), and the unique reads that fall within the targeted regions (unique on target) are shown. (*B*) The sequence coverage of targeted bases. The fraction of the targeted bases that were covered by unique reads at the sequence depth of 1×, 5×, 10×, and 20× is shown. (*C*) An overview of the somatic mutations identified by Exome-seq. Different markers and colors were used to show different mutation types. (*D*) The average number of somatic mutations identified per tumor cell line. (*E*) The performance of mRNA-seq in verification of somatic mutations identified by Exome-seq. The mutations that loci expressed represent those mutations that loci covered by five or more cDNA sequence reads. (*F*) Validation of the truncating mutations that introduced premature termination codons. The abundance of the mutant alleles in genomic DNA was compared with that of their corresponding cDNA.

of 1517 somatic mutations is shown in Supplemental Table S1. On average, each cell line contains 101 somatic mutations, 89% of which are base substitutions (Fig. 1D). The frequencies of mutant alleles ranged from 15%–100%, with a median of 41%. The depth of coverage at the mutation loci ranged from 10× to 637×, with a median of 42× (Fig. 1C; Supplemental Table S1). The lengths of somatic small indels varied from 1–29 bp. Seventy-eight percent of the indels were 1–3 bp in length (Supplemental Fig. S4). By using genome-wide SNP array, we identified more than 50 focal homozygous deletions (Supplemental Table S2). The *CDKN2A* locus at *9p21.3* and the *SMAD4* locus at *18q21.2* were frequently deleted in the tumor cell lines analyzed (Supplemental Fig. S5). The somatic mutations mainly clustered in nine signaling pathways, as shown in Supplemental Figure S6A. The background mutation rate estimated for targeted exonic regions was 2.7 mutations per megabase of DNA sequences.

Validation of somatic mutations using mRNA-seq

In total, 61.6% (934 out of 1517) of the mutations identified by Exome-seq were validated by mRNA-seq. If we focus on the expressed genes, 94.3% (914 out of 969) of the mutations at those loci covered by five or more cDNA sequence reads were successfully validated by mRNA-seq (Fig. 1E). Additionally, 20 mutations at the loci with a lower coverage (less than five reads, but three reads or more) were also confirmed by mRNA-seq. The percentages of mutations validated by mRNA-seq varied across mutation types. Generally, the validation ratio of truncating mutations is lower than that of nontruncating mutations.

For truncating mutations (Fig. 1F), the abundance of the mutant allele in the cDNA appears to be relatively lower than that of their corresponding genomic DNA (gDNA). Despite the lower abundance, mRNA-seq was still able to confirm 81 of those 94 (86.2%) truncating mutations at loci covered by five or more cDNA sequence reads. The remaining 13 truncating mutations were all heterozygous. Their loci were covered moderately well, but no mutant alleles were observed in the cDNA sequences. We performed Sanger sequencing to confirm if they resulted from the false-positive events of Exome-seq. As shown in Supplemental Figure S7, 12 of the 13 truncating mutations were successfully validated by Sanger sequencing. The mutant alleles were only detected in the gDNA of the tumor cell lines rather than in their cDNA, suggesting the transcripts carrying the mutant alleles were probably degraded through the nonsense-mediated mRNA decay (NMD) pathway (Holbrook et al. 2004). One mutation was found to be false-positive, possibly caused by mapping errors.

The recurrently mutated genes

In this study, 1359 genes were identified with somatic mutations. Among them, 56 genes were recurrently mutated in two or more cell lines (Table 2). The mutation rate of these genes was much higher than the background level. The most frequently mutated gene was *KRAS*, followed by *CDKN2A*, *TP53*, and *SMAD4*. Mutation of these four genes and 11 other genes has been reported either in the COSMIC database (http://www.sanger.ac.uk/genetics/CGP/cosmic/) or in a previous study (Jones et al. 2008), as shown in Supplemental Figure S8, while mutation of the remaining 41 genes, to our knowledge, has not been described in PDAC. Totally, 150 point mutations were identified in the 56 recurrently mutated genes. Among them, 109 mutations in 40 genes were confirmed by mRNA-seq (Supplemental Table S1). For the remaining 41 mutations that were not confirmed by mRNA-seq, seven loci were poorly expressed (covered by two or fewer cDNA sequence reads) and 34 loci were not expressed at all.

Table 2. The recurrently mutated genes

Rank	#Gene symbol	Coding sequence length (bases)	Number of point mutations	Number of DNA copy number variants	Number of deleterious mutations	Normalized mutation rate (mutions/Mb)	Tumor cell lines: PA028T	PA086T	PA090T	PA107T	PA122T	PA182T	PA195T	PA215T	PA254T	PA333T	PA018T	PA055T	PA167T	PA202T	PA285T
1	*KRAS*	570	16	7	15	1754.4	S		L	A				A			A	A	A	L	
2	*CDKN2A*	471	1	12	10	1415.4		L	P		L						L				
3	*TP53*	1182	12	14	12	676.8	L	L		L	L	L	L	L	L	L	L	L	L	L	L
4	*SMAD4*	1659	4	11	8	321.5	L					L	L	L	L	L					L
5	***PDCD6***	576	2	4	2	231.5	A							A	A				A		
6	***IL1B***	810	2	1	2	164.6													A		
7	***FAM92B***	915	2	3	2	145.7	A							L					A		
8	*OR4L1*	939	2	3	2	142.0				L		L				L					
9	***SFXN4***	1014	3	1	2	131.5						L									U
10	***RNF207***	1905	3	2	3	105.0	L		L												
11	***ASL***	1395	2	1	2	95.6	A														
12	***TYSND1***	1701	2	2	2	78.4					L				L						
13	***ACSM1***	1734	2	3	2	76.9	L							L					A		
14	***NFE2L2***	1818	2	1	2	73.3													A		
15	*PTPRD*	5739	3	14	6	69.7	P	L	L	P	L	L	L		P	L	L	L	P	L	SL
16	***CCDC41***	2106	2	6	2	63.3			L	L			L	L			L	L			
17	***EXOC8***	2178	2	-	2	61.2															
18	***CLCN4***	2283	2	3	2	58.4	L							L						L	
19	*KIAA1751*	2289	2	1	2	58.2			L												
20	***SOX5***	2292	2	5	2	58.2				A			A	A				A	A		
21	***WDR75***	2493	2	-	2	53.5															
22	***SAGE1***	2715	2	4	2	49.1	L			L								L		L	
23	*GRM8*	2727	2	2	2	48.9					L			L							
24	***TMTC3***	2745	2	8	2	48.6			L	L	L		L	L		L	L	L			
25	***CNTNAP1***	4155	4	3	3	48.1				L			L						L		
26	***ABCC5***	4314	3	1	3	46.4				M			A								
27	***CARD10***	3099	3	5	2	43.0	L			L									L	L	ML
28	***PEAR1***	3114	2	-	2	42.8															
29	***FUK***	3255	2	2	2	41.0												L	A		
30	***SORCS1***	3597	2	6	2	37.1					L	L	L		L		L	L			
31	***GIGYF2***	3963	2	1	2	33.6				L											
32	*CNTNAP2*	3996	2	1	2	33.4															
33	***CLIP1***	4284	2	5	2	31.1			L	L				L			L	L			
34	***MYOM3***	4314	2	3	2	30.9	L		L	L											
35	***LPHN1***	4425	2	4	2	30.1	L			L				L				L			
36	***CDC42BPB***	5136	3	3	2	26.0						L	A			L					S
37	***AKAP11***	5706	2	6	2	23.4	L					A		L			L	L	L		
38	***MYH4***	5820	2	10	2	22.9	L	L				L	L	L		L	L	L	L	L	
39	***EXPH5***	5970	2	1	2	22.3						L									
40	***PHF3***	6120	2	3	2	21.8	L										L	L			
41	***CDC42BPG***	6597	2	4	2	20.2		L		L							A		L		
42	*ARID1A*	6858	2	4	2	19.4	L		L	L						L					
43	***SON***	7281	2	2	2	18.3								L				L			
44	*MLL3*	14736	4	5	4	18.1	A				L			L				L	L		
45	***IGF2R***	7476	2	6	2	17.8	L						L		L		L	L		L	
46	***IGSF10***	7872	2	2	2	16.9							A				A				
47	***UTP20***	8358	2	6	2	16.0			L	L	L		L	L				L			
48	*VWF*	8442	4	4	2	15.8				A			A				A	A			S
49	***AKAP13***	8454	2	1	2	15.8												L			
50	*BRCA2*	10257	3	4	2	13.0	L							L			L	L	L		
51	*ALMS1*	12504	2	1	2	10.7							A								
52	***FAT2***	13050	2	2	2	10.2							L								L
53	***USH2A***	15609	2	1	2	8.5											L				
54	***MACF1***	16293	2	-	2	8.2															
55	***HMCN1***	16908	2	-	2	7.9															
56	*DNAH9*	17896	2	9	2	7.5	L	L				L	L	L			L	L	L		L

#Gene symbol, the genes colored in orange indicate those genes in which mutations have been described previously in PDAC.

Missense Nonsense Synonymous Frame-shift indel
Homozygous deletion (the entire gene) Homozygous deletion (part of the gene)
L: LOH A: Amplification M: +1 Missense S: +1 Synonymous U: +1 substitution in UTR

The widely varied mutation rates

Exome-seq revealed that the mutation rates varied significantly among cell lines (Figs. 2C, 3A). The number of somatic substitutions identified from each cell line ranged from 31–640, and the number of somatic indels varied from zero to 100. Accordingly, we classified the cell lines into three subgroups. Cell lines in group 1 ($n = 10$) showed a modest level of somatic mutations, while cell lines in group 2 ($n = 4$) showed a significantly elevated rate of small indels ($P = 0.005$) (Fig. 2C); a cell line in group 3 ($n = 1$) showed dramatically increased rates of both indels and substitutions (Figs. 2C, 3A). In the group-3 cell line, we observed a much higher prevalence of mutations involved in all nine core signaling pathways ($P = 0.0007$) (Supplemental Fig. S6B). In group-2 cell lines, the normalized mutation rate was slightly but significantly increased ($P = 0.037$) in seven of the nine pathways.

Allelic loss of *MLH1* and the increased mutation rate

To find out the genetic factors that accounted for the increased mutation rate in the group-2 and group-3 cell lines, we first screened the MMR genes for somatic alterations. We found that the

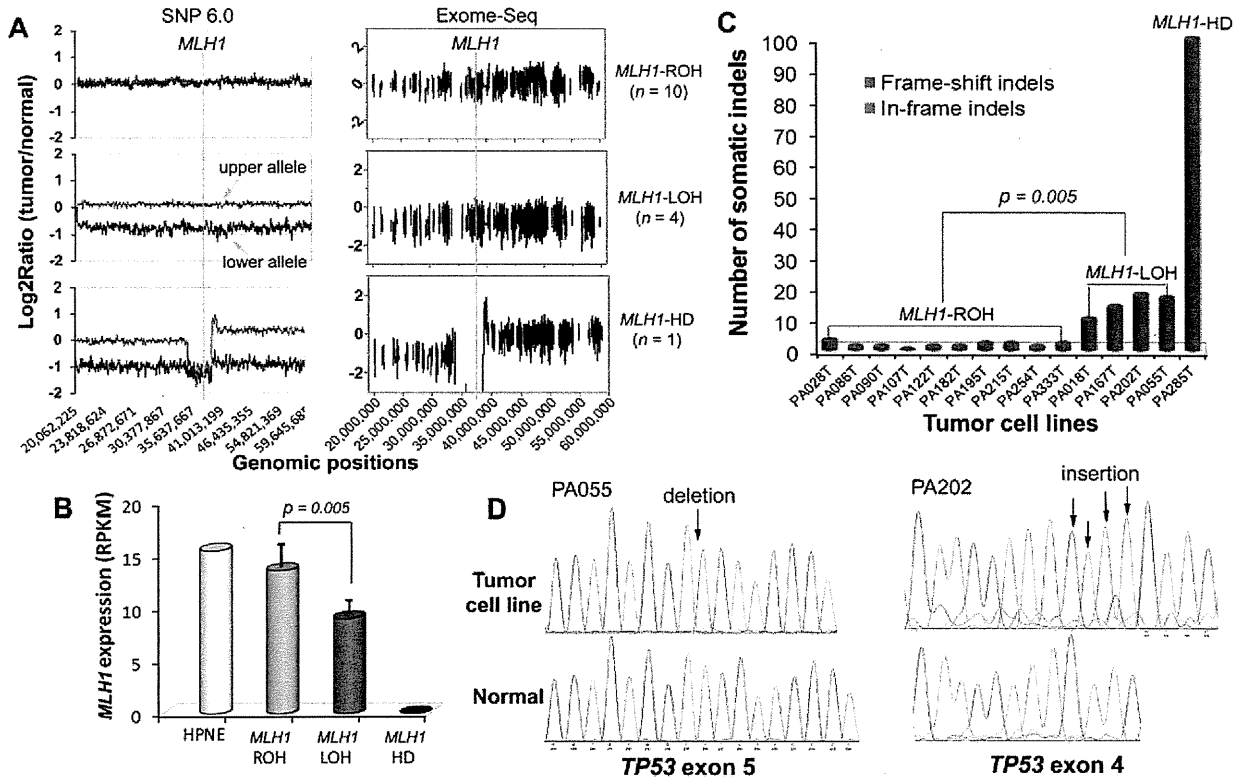

Figure 2. Allelic loss of *MLH1* and the increased rate of somatic indel mutations. (*A*) The distinct DNA copy-number status of *MLH1*. The *left* and *right* panels show the DNA copy-number status inferred from SNP array and Exome-seq data, respectively. The line in light blue indicates the approximate genomic location of *MLH1*. For graphs in the *left* panel, the *y*-axis indicates the adjusted $\log_2$ ratios of signal intensities between the tumor cell line and its matched normal sample for perfect match probes. The red line represents the allele with a higher copy number, and the blue line represents the allele with a lower copy number. The $\log_2$ ratio of −1 and 0 theoretically corresponds to 0 and 1 copy, respectively. For graphs in the *right* panel, the *y*-axis indicates the $\log_2$ ratios of the sequence coverage between the tumor cell line and its matched normal sample for targeted exonic regions. (*B*) The differential expression of *MLH1*. The gene expression level was examined by mRNA-seq. (*RPKM*) Reads per kilobase per million mapped reads. (Bars) Mean ± SD. (*C*) The somatic indels. The number of somatic small indels identified in the targeted exonic regions is shown for each tumor cell line. (*D*) Validation of the truncating indels identified in *TP53* in two *MLH1*-LOH cell lines. (*Left*) 1-bp deletion; (*right*) 4-bp insertion. The positions of indels are indicated by arrows in the sequence electropherograms.

gene *MLH1* was differentially expressed among the subgroups, and the expression levels appeared to be reversely correlated with the mutation rates. As shown in Figure 2B, the expression of *MLH1* decreased by nearly half in group-2 cell lines ($P = 0.005$) and was almost lost in the group-3 cell line. We did not observe any significant differences in the expression of other DNA MMR genes among the subgroups (Supplemental Fig. S9), nor did we detect somatic point mutations of other MMR genes in any of the cell lines. We then quantitatively measured the methylation status of the *MLH1* promoter using MassARRAY, but none of the cell lines showed promoter hypermethylation of this gene (Supplemental Fig. S10). We further examined DNA copy-number changes of *MLH1* and found a clue to its differential expression. As shown in the left panel of Figure 2A, cell lines in group 1 retained both alleles of *MLH1* (*MLH1*-ROH [retention of heterozygosity]), while cell lines in group 2 lost one of the two alleles of this gene (*MLH1*-LOH [loss of heterozygosity]); the cell line in group 3 lost both alleles (*MLH1*-HD [homozygous deletion]). The distinct DNA copy-number status of *MLH1* was also well demonstrated by the read-depth–based Exome-seq data (Fig. 2A, right panel).

Characterization of somatic indels in the *MLH1*-LOH and *MLH1*-HD cell lines

We identified an average of 1.4 ± 0.8 indels per *MLH1*-ROH cell line, 14.8 ± 3.5 indels per *MLH1*-LOH cell line, and 100 indels in the *MLH1*-HD cell line. The mutation rate of the somatic indels was 10.5- and 72.1-fold higher in *MLH1*-LOH and *MLH1*-HD cell lines, respectively, compared with that of the *MLH1*-ROH cell lines ($P = 0.005$) (Fig. 2C). Among the total of 173 somatic indels, 94 were detected in the coding microsatellites (Supplemental Table S1). Prevalence of the indels in the microsatellites was increased sixfold and 154-fold, respectively, in the *MLH1*-LOH and *MLH1*-HD cell lines. Nearly half of the indels that were detected in *MLH1*-LOH cell lines and the majority of indels that were detected in the *MLH1*-HD cell line were frame-shift mutations. Some of the frame-shift indels were present in cancer-related genes such as *TP53*, *BRCA2*, *TGFBR2*, and *MLL3* and were predicted to be protein truncating. We identified a 1-bp insertion in the poly(A)10 tract of *TGFBR2* in one of the *MLH1*-LOH cell lines and validated it by mRNA-seq. We detected two truncating indels in *TP53* in two other *MLH1*-LOH cell lines and validated them by both Sanger sequencing

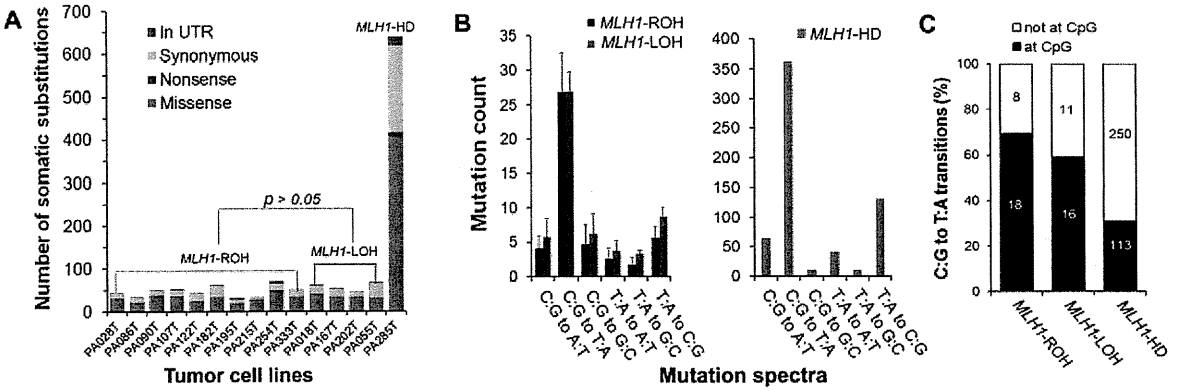

Figure 3. Characterization of the somatic base substitutions. (*A*) The number of somatic base substitutions. The *MLH1*-HD cell line showed a dramatically elevated mutation rate of somatic substitutions. (*B*) The pattern of mutation spectra. (*C*) The distribution of the C:G to T:A transitions at and not at the CpG dinucleotides. For *B*, the data are shown as mean ± SD. As for *C*, the mean values are marked on corresponding columns.

and mRNA-seq (Fig. 2D; Supplemental Table S1). Both indels were accompanied by LOH and introduced premature termination codons (PTCs), resulting in a dramatic reduction of *TP53* expression (Supplemental Fig. S11).

The mutation spectra

The pattern of mutation spectra was quite similar among the subgroups. As shown in Figure 3B, the predominant type of base substitution was the C:G to T:A transition, followed by the T:A to C:G transition. Many cancer genes such as *KRAS*, *TP53*, *SMAD4*, and *APC* were mutated by a C:G to T:A transition. In the *MLH1*-HD cell line, the mutation rate of the C:G to T:A transitions was markedly increased, especially at non-CpG sites (Fig. 3C). The frequency of other classes of base substitution was also dramatically higher except for the C:G to G:C and T:A to G:C transversions.

Evaluation of genomic instability using Exome-seq

Based on the Exome-seq data, we determined the microsatellite instability (MSI) status of *MLH1*-ROH, *MLH1*-LOH, and *MLH1*-HD cell lines as "stable," "intermediately unstable," and "highly unstable," respectively (Supplemental Table S1). We then performed the conventional MSI assay for the same sample set (Supplemental Fig. S12). The assay revealed that all seven markers were stable in the *MLH1*-ROH cell lines, and two of the markers, D17S250 and D2S123, were unstable in the *MLH1*-HD cell line. However, none of the markers showed instability in any of the *MLH1*-LOH cell lines. Using the conventional MSI assay, *MLH1*-LOH cell lines were indistinguishable from *MLH1*-ROH cell lines. To further evaluate the performance of Exome-seq, we selected three representative coding microsatellites, within which somatic indels have been identified by Exome-seq and validated by mRNA-seq. We designed fluorescence-labeled primers and performed the MSI assay. The conventional assay confirmed instability for all three microsatellites (Fig. 4).

Discussion

In this study, we analyzed 15 PDAC-derived cell lines and their matching normal tissues using Exome-seq. We detected more than 1500 point mutations and showed that 1359 genes were somatically altered in at least one of the cell lines. *KRAS*, *TP53*, *CDKN2A*, and *SMAD4*, known as the "master" genes for PDAC, were the top four most frequently mutated genes identified in this study. These results are consistent with an early study performed by Jones and colleagues (2008) using the Sanger sequencing method, indicating a good performance of Exome-seq, as well as our mutation detection pipeline.

Mutation of the four key players, although being of paramount importance, may not be sufficient to drive the development and progression of PDAC, since variability can occur among tumors arising in the same organ and among cell populations within the same tumor. Recent studies have reported the intertumoral heterogeneity among PDACs and the intratumoral heterogeneity in a hepatocellular carcinoma (Kim et al. 2011; Totoki et al. 2011). The number of mutated genes that drive development of cancer was found to be far greater than previously thought (Greenman et al. 2007). By using Exome-seq, we identified additional 52 genes that recurrently mutated in PDAC. Among them, the mutation of 41 genes has not been described in this cancer type. More than half of these genes have been suggested to play a role in carcinogenesis. For example, a recent study showed *NFE2L2* is frequently mutated in lung cancers (Shibata et al. 2010). The overexpression of *SOX5* is associated with prostate tumor progression and early development of distant metastasis (Ma et al. 2009). *EXOC8* has been shown to foster oncogenic Ras-mediated tumorigenesis (Issaq et al. 2010). Mutation screening of these genes in a large sample size would help us gain a further understanding of their biological contribution to PDAC.

The application of NGS technologies to cancer genomics has dramatically increased the efficiency of mutation discovery. Since a variety of factors, such as sequencing platforms, data mapping, and variant calling algorithms can affect the final output of identified mutation candidates, validation of the numerous proposed mutations has consequently become a common issue to be considered. We here evaluated the performance of mRNA-seq in verification of mutations identified in coding regions. If we simply consider all somatic mutations identified by Exome-seq, 61.6% of them were validated by mRNA-seq. If we focus, however, on those mutations in expressed genes, 94.3% of them can be successfully confirmed by mRNA-seq. For truncating mutations, despite a lower abundance of the mutant allele in cDNA, mRNA-seq was still able to confirm 86.2% of the mutations. This suggests that although it may miss mutations in poorly expressed regions, mRNA-seq may

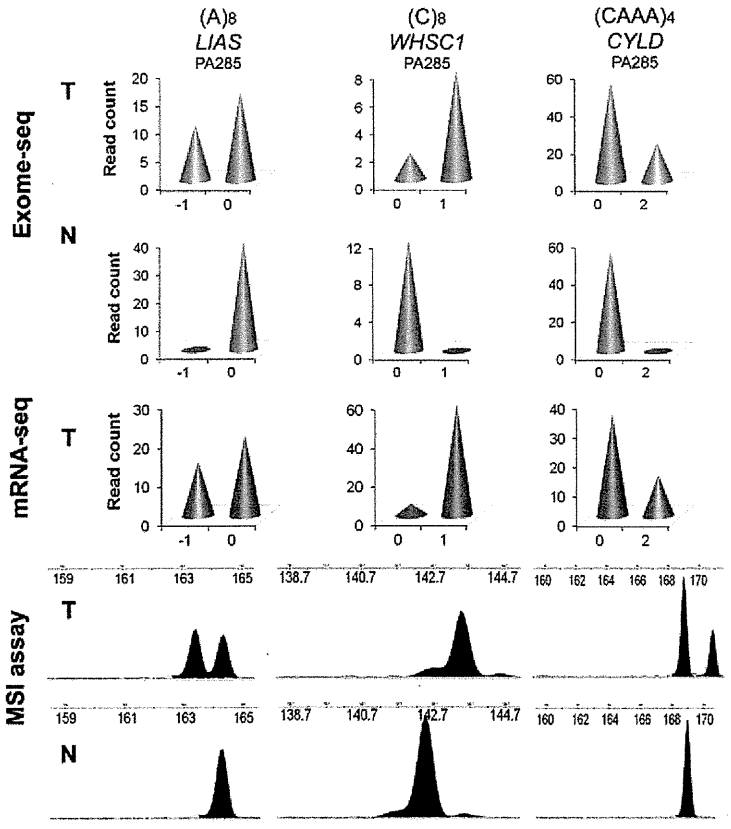

Figure 4. MSI analysis using Exome-seq. The data for three representative microsatellites are shown. (*Top*) Read-depth based Exome-seq data; (*middle*) mRNA-seq data; (*bottom*) electropherograms of the conventional MSI assay. For the *top* and *middle* panels, the *x*-axis indicates the lengths of indels. The negative value indicates base deletion, and the positive value indicates base insertion, while 0 indicates no indel. The numbers marked at the *y*-axis indicate the number of sequence reads that carry the mutant allele or the wild-type allele. (*Bottom*) *x*-axis is the size in bases; *y*-axis is the fluorescence intensity. The red peaks are internal size standards.

be a workable alternative to Sanger sequencing for the validation of mutations identified in expressed genes. In addition to learn about gene expression and splicing variants, groups who run NGS on both gDNA and cDNA for the same sample set may get an extra benefit from such an application.

Allelic loss at the short arm of chromosome 3 is one of the most common genetic alterations observed in human cancers. It has been reported in over 30% of PDAC and nearly 90% of RCC cases (Yamano et al. 2000; Harada et al. 2008; Toma et al. 2008). Many potential cancer genes have been identified on chromosome 3p. The DNA MMR gene *MLH1* is located at chromosome 3p22.2. In mammals, the MLH1 protein is an essential component of the MMR complex. MLH1 protein binds to either PMS1 or PMS2, and both heterodimers bind either to the MSH2/MSH6 heterodimers to correct mismatches or to the MSH2/MSH3 heterodimers to correct indel errors (Jiricny 1998; Kolodner and Marsischky 1999; Raschle et al. 1999). Among the MMR proteins, the loss of MLH1 is by far the most common cause of MSI. To date, a variety of genetic and epigenetic alterations in *MLH1* has been discovered in many different types of cancers (Bronner et al. 1994; Cunningham et al. 1998; Kuismanen et al. 2000; Suter et al. 2004; Arnold et al. 2009). In pancreatic cancers, the mutation of *MLH1* and MSI has been reported in a histologically distinct subset of poorly differentiated adenocarcinomas, called medullary carcinomas, which usually have a wild-type *KRAS*. The sporadic PDAC, however, seldom, if ever, has MSI (Wilentz et al. 2000). To our knowledge, the profile of MSI has yet to be fully demonstrated in a genome-wide manner in pancreatic cancers.

Homozygous deletion of *MLH1* is a rare case and has not been documented previously. In one of the cell lines analyzed in this study, we incidentally detected a focal homozygous deletion spanning the entire *MLH1* locus. Exome-seq revealed intensive genomic instability in this cell line, indicated by a dramatically elevated mutation rate of somatic substitutions, small indels, as well as the indels presented in coding microsatellites. The number of C:G to T:A transitions was markedly increased, especially at non-CpG sites, suggesting an impaired recognition/repair of G:T mismatches (Marra and Schar 1999; Kumar et al. 2009). The mutation spectrum of the cell line was quite similar to that of other types of MMR-deficient tumors previously reported (Greenman et al. 2007).

Although allelic loss of *MLH1* has been reported in over 30% of PDACs (Yamano et al. 2000; Harada et al. 2008), no statistical correlation has been described between *MLH1* allelic loss and an increased mutation rate. It was previously thought that mutations in *MLH1* and other DNA MMR genes are recessive; i.e., a single copy of the wild-type *MLH1* allele is sufficient to perform its normal function (Bodmer et al. 2008; Negrini et al. 2010). In this study, we notably found that *MLH1* expression was decreased by nearly half in cell lines with an allelic loss of *MLH1*. While these cell lines were negative in a conventional MSI assay, they showed a 10.5-fold increase in the rate of somatic indels. We also observed a higher prevalence of indels in the coding microsatellites. Moreover, we identified truncating indels that inactivate tumor suppressor genes, such as *TP53* and *TGFBR2*. These results indicate that deletion of one copy of *MLH1* gene results in haploinsufficiency in the correction of DNA indel errors.

An earlier study performed in vitro could support our argument that hemizygous deletion of *MLH1* may lead to an impaired DNA repair and genomic instability. Edelmann and colleagues (1996) generated mice with a null mutation of the *MLH1* gene and measured the MMR activity in vitro using the cell-free extracts from the mouse embryo-derived fibroblast (MEF). They found that the embedded errors in the reporter gene were repaired 2.3-fold less efficiently in MEF extracts of $mlh1^{+/-}$ mice compared with that of $mlh1^{+/+}$ mice.

To further address the significance of *MLH1* hemizygous deletion in in vivo tumors, we examined the primary RCC samples, which usually exhibit LOH on chromosome 3p. All patients provided informed consent for the research use of their samples, and

the study was approved by the institutional review board of the National Cancer Center Research Institute. We enriched the exonic sequences of 15 primary RCCs and their matched normal samples using the Agilent Human All Exon 50 Mb Kit and sequenced the exomes using the HiSeq 2000 sequencing system. Among the 15 RCCs analyzed, 13 cases showed LOH at the *MLH1* locus on chromosome 3p, and two cases showed ROH. The data are shown in Supplemental Figure S13 and Supplemental Table S3. On average, we identified 1.5 somatic indels in the *MLH1*-ROH cases, which is consistent with a previous report (Varela et al. 2011). However, in the *MLH1*-LOH tumors, we observed a 4.6-fold increased rate of somatic indel mutations ($P = 0.0008$). A total of 90 somatic indels were identified in 13 *MLH1*-LOH cases. Among them, 85 were frame-shift indels and 68 were truncating indels. Moreover, we detected recurrent truncating indels in several well-characterized cancer genes, such as *VHL* (four cases), *PBRM1* (four cases), and *JARID1C* (four cases). These data suggest that the correlation we observed between *MLH1* allelic loss and the increased mutation rate of somatic indels is more likely to be the true rather than a simple coincidence. Our data also indicate that *MLH1* allelic deletion, through increasing the frequency of somatic indel mutations in cancer genes, could drive the development and progression of cancer. It is potentially significant that the correlation we observed was only with somatic indels, and not base substitutions. Presumably, MLH1 protein may play a pivotal role in correction of DNA indel errors, while its function for MMR can be partially compensated by other MMR proteins or mechanisms. Nevertheless, we could not exclude the possibility that factors that predispose to DNA copy-number losses might also associate with indel frequency.

In human cancers, LOH at chromosome 3p is frequently observed (Yamano et al. 2000; Harada et al. 2008; Toma et al. 2008). However, the association between *MLH1* allelic loss and the increased rate of somatic indel mutations has not been notified. There are several possible reasons. First, depending on the platform, sequencing indels can be difficult. Second, reads arising from indel sequence are generally more difficult to be aligned to the reference genome. Without a good coverage, indels are more difficult to be detected. Third, the MSI assay is conventionally used to evaluate the occurrence of indels at microsatellites as genome-wide mutation analysis was not available until recently (Boland et al. 1998). The MSI assay is insufficient since only several microsatellites are selected. In addition, technical limits exist in the conventional assay (Hatch et al. 2005; Fujii et al. 2009). For example, the assay system employs capillary electrophoresis and autoradiography, making it sometimes difficult to recognize small changes in the microsatellite sequences. Some artificial fragment peaks were usually introduced after 32 cycles of PCR amplification. The choice of markers may also affect the sensitivity of the assay (Hatch et al. 2005; Fujii et al. 2009). In contrast, our data suggest that Exome-seq may be an acceptable alternative for microsatellite analysis.

Methods

The samples

PDAC-derived cell lines

We analyzed a total of 15 PDAC-derived cell lines and their matched normal samples. Primary pancreatic tumor tissue contains a high admixture of contaminating non-neoplastic inflammatory and stromal cells. To remove the non-neoplastic cells and facilitate the detection of somatic mutations, microdissected primary tumors were passaged in vitro as cell lines prior to extracting DNA and RNA for sequence analysis. The characteristics of the PDAC-derived cell lines are listed in Table 1. All cell lines were established by researchers at the Cancer Institutes, Japanese Foundation of Cancer Research (JFCR). The matching normal tissues were surgically resected from tumor-negative pancreas. All normal samples were histologically reviewed by two pathologists and were confirmed to be free of tumor tissues. All patients provided informed consent for the research use of their samples, and the study was approved by the institutional review board of the JFCR and the University of Tokyo. The DNA and RNA were extracted by standard protocols. The pair matching of each tumor cell line and the normal sample was confirmed by genome-wide SNP array (Affymetrix).

HPNE cell line

The human telomerase reverse transcriptase (hTERT)-immortalized pancreas duct epithelial cell line (hTERT-HPNE, CRL-4023) was purchased from The American Type Culture Collection (ATCC). The cells were cultured in low-glucose DMEM media (Invitrogen) supplemented with 25% Medium M3 Base (Incell), 5% fetal bovine serum, and 10 ng/mL human recombinant epithelial growth factor (Sigma Aldrich) at 37°C and with 5% carbon dioxide. HPNE serves as the normal control for gene expression analysis.

Exome-seq and data analysis

Exome-seq

Targeted enrichment was performed with Agilent SureSelect Human All Exon Kit V1.0 (Agilent Technologies). This kit is designed to enrich 162,073 exons of 16,954 protein-coding genes, more than 700 microRNAs and 300 noncoding RNAs, covering ~37.6 Mb of the human genome (Supplemental Fig. S14). SureSelect Biotinlyated RNA baits were designed to be 120-mer long and end-to-end tiled (1× tilling). The gDNA libraries were prepared using an Illumina paired-end DNA sample prep kit (Illumina) following the manufacturer's protocols with slight modifications. In brief, 3 μg gDNA was fragmented using Covaris Acoustic Solubilizer (Covaris) with 20% duty cycle, 4 intensity, and 200 cycles per burst for 160 sec, at 16°C to get DNA fragments with a mean size of 200 bp. Fragmented DNA was then purified using Agencourt AMPure XP magnetic beads (Beckman Coulter). The concentration of the library was measured using a Bioanalyzer (Agilent Technologies). The adapter-ligated libraries were amplified with six PCR cycles, and 500 ng of each amplified library was hybridized with Biotinlyated RNA baits in solution for 24 h for target enrichment. Subsequently, hybridized libraries were cleaned up and further amplified with 12 cycles of PCR; 5–6 pM/lane DNA was applied to the flow cell, and paired-end 76-nucleotide (nt)-long reads were generated using the Illumina Genome Analyzer IIx Platform (GAIIx). Each sample was run on a single lane of Illumina flow cell except for samples PA028N and PA167T, which were each run on two lanes.

Data alignment and variant calling

The detail workflow for data alignment and mutation detection was described in Supplemental Figure S15. For each cell line and matched normal sample, the sequence reads were mapped to the human NCBI Build 36 reference sequence (hg18, downloaded from http://genome.ucsc.edu) initially with the Illumina sequencing pipeline (version 1.6) for quality recalibration. The passing filter (PF) reads were then mapped again using BWA (version 0.5.8) (Li and Durbin 2009). Any potential PCR duplicates, ambiguous reads, inconsistent read pairs, and singletons were excluded. Only the unique reads that mapped in consistent read pairs (with proper insert size and orientations) were selected for further